Multi-step loading of human Mini Chromosome Maintenance proteins in live human cells*

Ioanna-Eleni Symeonidou[1*], Panagiotis Kotsantis[1*#], Vassilis Roukos[1##], Maria-Anna Rapsomaniki[1], Hernán E. Grecco[2], Philippe Bastiaens[2], Stavros Taraviras[3] and Zoi Lygerou[1]

[1]Laboratory of General Biology and [3]Laboratory of Physiology, School of Medicine, University of Patras, 26500 Rio, Patras, Greece

[2]Department of Systemic Cell Biology, Max Planck Institute of Molecular Physiology, Otto-Hahn-Strasse 11, 44227 Dortmund, Germany

[*] I.E.S. and P.K. contributed equally to this work
[#]Present address: School of Cancer Sciences, College of Medical and Dental Sciences, Institute for Biomedical Research, University of Birmingham, Birmingham, B152TT, UK
[##]Present address: National Cancer Institute, National Institutes of Health, Bethesda, MD 20892, US

*Running title: Maximal loading of MCM2/4 in late G1

To whom correspondence should be addressed: Zoi Lygerou, Laboratory of General Biology, School of Medicine, University of Patras, 26500 Rio, Patras, Greece. Tel: (+) 30 2610 997610; Fax: (+) 30 2610 991769; E-mail: lygerou@upatras.gr

Keywords: Cell biology; Cell cycle; Chromatin; DNA replication; Imaging; Fluorescence Recovery After Photobleaching; Licensing; Live-cell imaging; Minichromosome Maintenance Complex; genome stability

Background: MCM2-7 loading onto chromatin licenses origins for replication.
Results: MCMs exhibit transient interactions with chromatin in late mitosis, stable binding in G1, and increased loading in late G1.
Conclusion: Multi-level regulation of MCM2-7 loading to chromatin occurs during mitosis and preceding the G1/S phase transition.
Significance: The dynamics of the DNA licensing system within live human cells reveal multiple control points.

SUMMARY

Once-per-cell cycle replication is regulated through the assembly onto chromatin of multi-subunit protein complexes which license DNA for a further round of replication. Licensing consists of the loading of the hexameric MCM2-7 complex onto chromatin during G1, and is dependent on the licensing factor Cdt1. *In vitro* experiments have suggested a two-step binding mode for MCM proteins, with transient initial interactions converted to stable chromatin loading. Here, we assess MCM loading in live human cells, using an *in vivo* licensing assay based on Fluorescence Recovery After Photobleaching (FRAP) of GFP tagged MCM protein subunits through the cell cycle. We show that in telophase, MCM2 and MCM4 maintain transient interactions with chromatin, exhibiting kinetics similar to Cdt1. These are converted to stable interactions from early G1 phase. The immobile fraction of MCM2 and MCM4 increases during the G1 phase, suggestive of reiterative licensing. In late G1 phase, a large fraction of MCM proteins are loaded onto chromatin, with maximal licensing observed just prior to S-phase onset. Fluorescence Loss In Photobleaching (FLIP) experiments show subnuclear concentration of MCM-chromatin interactions which differ as G1 progresses and do not co-localize with sites of DNA synthesis in S phase.

Faithful DNA replication is a prerequisite for the preservation of genomic information. In eukaryotic cells, DNA replication initiates from multiple replication origins distributed on chromosomes, which direct the assembly of multiprotein complexes (known as "replisomes"), which will move along with each replication fork

(1-4). The DNA replicated by sister forks from a single origin is called a replicon. It has been proposed that in eukaryotic cells the DNA replication machinery is restrained at specific nuclear structures called "replication factories", which exhibit dynamic behavior as they assemble and disassemble in space during S phase ((5-8), reviewed in (9,10)). Sister replication forks generated from the same origin are believed to remain associated within a replication factory while the entire replicon is replicated (11). Replication begins in nuclear euchromatin at approximately 100-300 foci (visualized after BrdU or PCNA staining) distributed throughout the nucleus. During mid S phase, these foci are located in heterochromatic regions near the nuclear periphery and surrounding the nucleoli, while in late S phase, only a few intense and larger replication foci are located at the nuclear periphery and within the nucleoli (6-10).

DNA replication must be limited to only once per cell cycle, so as to prevent re-replication and maintain genomic stability (reviewed in (12-14)). The integrity of genomic information is preserved through the periodic assembly and disassembly of essential pre-replication complexes (pre-RCs) at replication origins. This process, described as chromatin "licensing", involves the loading of the heterohexameric MCM2-7 (minichromosome maintenance) protein complex onto chromatin by the origin recognition complex (ORC) and two essential loading factors, Cdc6 (15) and Cdt1 (16,17). Licensing ensures the faithful regulation of DNA replication in time and space (18). The eukaryotic cell cycle is driven by the periodic activation and inactivation of cyclin-dependent kinases (CDKs) that allow pre-RC formation to occur in a time window between late mitosis through G1 phase, during which Cdk/cyclin levels are low due to the anaphase promoting complex/cyclosome (APC/C) and cyclin dependent kinase inhibitors (CKIs) (14). In metazoa, licensing is additionally controlled through Geminin (19), a protein which binds to Cdt1 and inhibits it from loading the MCM complex onto chromatin during S and G2 phases (20-22). The timing and extent of MCM loading onto chromatin must be accurately controlled through the cell cycle and co-ordinated with S-phase onset: both under-licensing and over-licensing have been linked to DNA replication stress, genomic instability and malignant transformation (23-25).

MCM2-7 proteins belong to the AAA ATPase family. They adopt a hexameric ring-like structure (26-28), large enough to accommodate ssDNA or dsDNA (27-30), and are considered the prime candidates for the eukaryotic replicative helicase (31). The spatial localization of MCMs after the onset of DNA replication, during which MCM proteins bind preferentially to unreplicated DNA, rather than to replicating or replicated DNA (32,33), as well as the excess number of MCM2-7 complexes loaded per ORC (34,35) raise questions on MCM function that are put together as the "MCM paradox". *In vitro* studies in yeast support a two-step model for the loading of the MCM2-7 complex onto chromatin (36-38). MCM proteins firstly bind transiently onto origin DNA and are then loaded stably in a step requiring ATP hydrolysis by cdc6 (39). The MCM2-7 complex is loaded in an inactive form at origins. As cells enter S phase the combined action of CDKs and Cdc7-Dbf4 (reviewed in (40)) leads to the formation of a complex between MCM2-7, Cdc45 and GINS (CMG complex) (41), which bears processive helicase activity (42) and is part of the replisome (43,44).

Live cell imaging studies revealed both ORC (45) and Cdt1 (46,47) to be highly mobile within the cell nucleus, while a recent study showed stable binding of MCM proteins throughout G1 and S phase in Chinese Hamster Ovary (CHO) cells (48). Here, we use live-cell imaging to assess MCM chromatin loading at different cell cycle stages of human cancer cells. Our analysis reveals transient interactions of MCM proteins with chromatin in telophase, followed by stable binding during G1. In addition, we show that in late G1 phase the fraction of MCM proteins which are bound to chromatin is markedly increased, suggesting that chromatin is only fully licensed in late G1. Our findings suggest multiple levels of regulation of MCM binding to chromatin within the live cell nucleus, taking place during both mitosis and at the G1 to S phase transition.

EXPERIMENTAL PROCEDURES

Cell culture, isolation of stable cell lines, cell synchronization and transfection, FACS analysis - MCF7 cells were grown in Dulbecco's modified Eagle's medium with 20% fetal bovine serum at

37°C and 5% CO_2. For live-cell experiments, cells were plated on MatTek dishes (MatTek Corporation) in phenol red-free, CO_2-independent medium (Invitrogen). Stable GFP-NLS, GFP-MCM2 and GFP-MCM4 cell lines were selected with 500 μg/ml Geneticin (Invitrogen). Stable Cdt1-GFP cell line generation and characterization have been previously described (47). For transient transfection, MCF7 cells plated in 35 mm dishes were transfected with a total of 1 μg of plasmid DNA for 24 hours using Lipofectamine 2000 (Invitrogen) or Turbofect (Fermentas) according to the manufacturer's instructions. For Cdt1 silencing, MCF7 stable cell lines were transfected with 400 nM of Cdt1 siRNA or control Luciferase siRNA using Lipofectamine 2000 twice, with a time interval of 24 hours and analyzed 48 hours following the second transfection.

For mitotic synchronization, cells were treated either with 40 ng/ml nocodazole (Sigma) for 12 hours or with 100 μM monastrol (Sigma) for 16 hours, collected by mechanical shake off and released into fresh medium. For late G1 synchronization, cells were grown in the presence of 0.5 mM mimosine (Sigma) for 24 hours. The synchronization in early S phase was performed with a double thymidine block (2.5 mM, Sigma) or with 5 mM Hydroxyurea (Sigma) treatment for 24 hours.

For FACS analysis, stable GFP-NLS, GFP-MCM2 and GFP-MCM4 cell lines, as well as parental MCF7 cells were fixed with 70% ice-cold ethanol and stained with propidium iodide (2 μg /ml) in the presence of 100 μg/ml RNase, in PBS. Cellular DNA content was analyzed using a Becton Dickinson flow cytometer with Cellquest software and WinMDi software version 2.8.

Immunofluorescence, Western blotting, Immunoprecipitation - Immunofluorescence was done as previously described (49). Primary antibodies used: α-MCM2 (BD Transduction) 1:500, α-MCM4 (BD Pharmingen) 1:600, α-Cdt1 (50) 1:250, α-Geminin (47) 1:250, α-Cyclin A (Neomarkers) 1:100. DNA was stained with Hoechst 33258 (Sigma), DAPI (Vector) or TOTO-3 (Molecular Probes).

For western blotting, total cell lysates were prepared by lysing cell pellets directly in SDS-PAGE loading buffer. Primary antibodies used: α-MCM2 (BD Transduction) 1:1000, α-MCM4 (BD Pharmingen) 1:6000, α-MCM7 (Santa Cruz) 1:500, α-Cdt1 (50) 1:250, α-GFP (Roche) 1:6000, α-tubulin (Sigma) 1:20000.

For immunoprecipitation experiments, total cell lysates from asynchronous MCF7 cells as well as from GFP-MCM2, GFP-MCM4 and GFP-NLS stable cell lines were prepared by using a lysis buffer containing 50 mM Tris-HCl pH 7.6, 150 mM NaCl, 5 mM EDTA, 5 mM $MgCl_2$, 0.5% Triton X-100, 1 mM phenylmethylsulfonyl fluoride and complete, EDTA-free Protease Inhibitor Cocktail Tablets (Roche). GFP-tagged proteins were immunoprecipitated using anti-GFP antibodies (mouse monoclonal anti-GFP, 3E6, 1181460001, Roche) bound to protein G agarose beads (Upstate). Immunoprecipitates were analyzed by western blotting.

Chromatin association assay - About $5x10^5$ cells were washed with ice-cold PBS buffer and lysed in 0.1 ml of 0.1% TX-100 mCSK buffer (10 mM Pipes, pH 7.9, 100 mM NaCl, 300 mM sucrose, 0.1 (v/v)% Triton X-100, 1 mM phenylmethylsulfonyl fluoride, 10 mM β-glycerophosphate, 1 mM Na_3VO_4, 10 mM NaF), for 15 minutes on ice. After centrifugation at 13,000 rpm for 15 minutes at 4°C, the supernatant that was isolated represented the soluble fraction (S100). The pellet was washed with equal volume of ice-cold 0.1% TX-100 mCSK buffer and suspended in SDS sample buffer (chromatin enriched fraction - P100).

Plasmids - To fuse GFP to the N-terminus of MCM2 and MCM4, the open reading frames of MCM2 and MCM4 (kindly provided by Dr. A Perrakis) were subcloned into pCDNA3.1/EGFP (Invitrogen) between the EcoRI and XhoI sites. PCNA tagged to mRFP (PCNA-RFP) was kindly provided by Dr C. Cardoso (51). A GFP-nls construct was generated by cloning three copies of the SV40 nuclear localization sequences at the C-terminus of the GFP sequence in pEGFP-C1 vector.

Photobleaching experiments and analysis – Photobleaching experiments were performed on a Leica TCS SP5 confocal microscope equipped with a 63x 1.4 NA oil immersion lens. During experiments cells were maintained at 37°C and 5% CO_2. For Fluorescence Recovery after Photobleaching (FRAP) experiments, bleaching was accomplished on a defined region of interest of 2 μm diameter, within the cell nucleus. Fifty prebleach images were recorded with 3% laser

power of the 488 nm line at 70% argon laser intensity and bleaching was attained by a double bleach pulse of 0.066 seconds using the 458, 476, 488 and 496 nm laser lines combined at maximum power. Following bleaching, 250 images were recorded at 0.066 seconds intervals with 3% laser power of the 488 nm line. Raw data were normalized as previously described (47). Immobile fractions and $t_{1/2}$ values were extracted after a double exponential fitting using the program easyFRAP (52) and the FRAPcalcV9j application of Dr Kota Miura (EMBL).

Fluorescence Loss in Photobleaching (FLIP) experiments were performed by repeatedly bleaching a specified region within the cell nucleus. In Figures 7A, a circular region of 4 μm in diameter within the cell nucleus was repeatedly bleached with 60 pulses using the 458, 476, 488 and 496 nm laser lines combined at maximum power, In figure 7C a region corresponding to approximately 1/3 of the nucleus was bleached as above. In Figure 7B, about 1/3 of the cell nucleus was bleached with 150 pulses using the 476 and 488 nm laser lines combined at 70% laser intensity using a FRAP-booster (Leica TCS SP5 Confocal Microscope). Following FLIP, confocal images were recorded to visualize immobile structures of GFP-MCM2 within the nucleus. In Figure 8, the redistribution of fluorescence was monitored by acquiring a series of 10 optical sections along the z axis of each cell, at 5-minute intervals over a period of 2 hours.

Quantification and image analysis - siRNA-mediated depletion of Cdt1 was estimated by quantifying mean fluorescence intensities of cells subjected to immunofluorescence with anti-Cdt1 antibody using ImageJ 1.37g (Wayne Rasband, National Institute of Mental Health, Bethesda, MD).

For each cell subjected to FLIP in Figure 8, the maximum projection of the z-stacks was quantified and a linear filter was applied to remove noise and smoothen the image, by setting the intensity value of each pixel to the average of the pixels in its 6 x 6 neighbourhood. The corresponding data are shown as mesh plots. The analysis was performed using MATLAB R2007b.

RESULTS

A system for studying MCM protein dynamics within live human cells - In order to study the dynamics of MCM proteins within live human cells, the MCM2 and MCM4 proteins were fused to green fluorescent protein (GFP) at their N-termini (GFP-MCM2 and GFP-MCM4). MCM4 was chosen as it was shown to interact with the GINS complex (42) and its phosphorylation by Cdc7 facilitates the interaction with Cdc45 on chromatin (53). MCM2, as well as MCM3, carry nuclear localization sequences (NLS) sequestering the other MCM subunits to the cell nucleus (54). The GFP-MCM2 and GFP-MCM4 constructs, under the control of the constitutive CMV promoter, were used for transient expression in MCF7 human breast cancer cells. GFP-MCM2 localized to the nucleus and was excluded from the nucleoli, similar to endogenous MCM2 (data not shown). GFP-MCM4 transiently expressed showed both nuclear and occasional cytoplasmic localization (data not shown), consistent with previous results showing that MCM4 lacks a nuclear localization signal and is transported to the nucleus in complex with other subunits (48,54). Several MCF7 cell lines stably expressing GFP-MCM2, GFP-MCM4 or a nuclear localized construct of GFP (GFP-NLS) were generated and analysed by GFP fluorescence and western blot analysis (data not shown). Clonal cell lines expressing the tagged proteins at levels similar to the endogenous MCM2 and MCM4 respectively were selected for further analysis (Figure 1A). In figures 1B and 1C, GFP fluorescence in the stable cell lines is compared to immunofluorescence using anti-MCM2 and anti-MCM4 specific antibodies. Both GFP-MCM2 (Figure 1B) and GFP-MCM4 (Figure 1C) exhibited the same subcellular localization as the endogenous proteins, localizing to the nucleus and being excluded from the nucleoli. This analysis further verified the low-level expression of the tagged moieties, as no increase in total anti-MCM2 and anti-MCM4 staining was observed in the stable cell lines, and indicated correct complex formation of GFP-MCM4 expressed to low levels, allowing its correct localization to the nucleus. To verify that the constitutive expression of the tagged MCM2 and MCM4 moieties, even at low levels, did not interfere with correct cell cycle progression, the cell cycle profiles of the stable cell lines were compared to the parental MCF7 cell line. Fluorescence-activated cell sorter (FACS) analysis of the stable cell lines produced

cell-cycle profiles similar to the parental MCF7 cells (Figure 1D). This finding was further confirmed by immunofluorescence against different cell-cycle markers: the percentage of cells in GFP-MCM2, GFP-MCM4 and GFP-NLS expressing cell lines which were positive for Cdt1 (G1 marker), Geminin (S-G2 marker) and Cyclin A (S-G2 marker) was similar to those of the control MCF7 cells (Figure 1E).

We then addressed whether GFP-MCM2 and GFP-MCM4 were able to interact and form complexes with the other endogenous MCM subunits of the MCM2-7 hexamer. Total cell extracts from GFP-MCM2, GFP-MCM4 and GFP-NLS (as negative control) stable cell lines were immunoprecipitated using an anti-GFP antibody and immunoprecipitates analyzed by western blotting using specific antibodies for MCM2, MCM4 and MCM7. As shown in figure 1F, both GFP-MCM2 and GFP-MCM4 form complexes with the other endogenous MCM subunits.

To assess the ability of GFP-MCM2 and GFP-MCM4 to associate with chromatin during the cell cycle, chromatin association assays were performed in mitotically synchronized cell populations. Cells were arrested in mitosis by nocodazole and mitotic shake-off, and time-points taken following release, as cells progressed synchronously in G1. As shown in figure 2A, GFP-MCM2, similar to endogenous MCM2, is expressed in mitosis and throughout G1, but associates with a chromatin enriched insoluble fraction following release into G1, in parallel to the chromatin association of Cdt1. Note the hypermodification of Cdt1 in mitotically arrested cells, as previously reported (55). Similarly, GFP-MCM4 associated with chromatin during the G1 phase, with kinetics similar to the endogenous MCM4 (Figure 2B). Note the hypermodification of both the endogenous MCM4 and GFP-MCM4 in mitosis (as previously reported (56)), and the apparent decrease in their protein levels at the mitotic block, which point to regulation of MCM4 in mitosis by post-translational modifications and proteolysis. Note also that Cdt1 chromatin association temporarily precedes MCM2 and MCM4 chromatin association. These experiments confirm that both GFP tagged proteins associate with chromatin with kinetics similar to the endogenous ones.

Taken together, the above results show that GFP-MCM2 and GFP-MCM4 functionally mimic the behavior of their endogenous counterparts, allowing their use for the investigation of the spatiotemporal regulation of the endogenous proteins in live human cells.

Fluorescence recovery after photobleaching reveals an immobile MCM pool within the live-cell nucleus - Our previous work had shown that Cdt1-GFP exhibits a scanning behavior during the G1 phase of human cultured cells, maintaining dynamic short-lived interactions with chromatin throughout G1 (47). A similar dynamic behavior was also reported for Origin Recognition Complex (ORC) components (45). In contrast, a recent study showed stable binding of MCM proteins to chromatin in CHO cells (48). To investigate the behavior of MCM proteins in live human cells, real-time *in vivo* confocal fluorescence microscopy was used. Unsynchronized MCF7 cells stably expressing GFP-MCM2, GFP-MCM4 and GFP-NLS were subjected to Fluorescence Recovery after Photobleaching (FRAP). In parallel, MCF7 cells stable for Cdt1-GFP were analyzed for comparison (47). The mobility and kinetic properties of MCM2, MCM4 and Cdt1 were assessed by photobleaching the GFP tagged proteins in a small circular region (2 μm in diameter) located inside the nucleus and then monitoring the recovery of fluorescence over time. Mean normalized curves derived from 15-50 individual cells are shown in figure 3. Curve fitting of all individual recovery curves (52) was used to calculate the half-time ($t_{1/2}$) of the fluorescence recovery and the fraction of molecules which were immobile (Imm. Frac.). Both MCM2 and MCM4 displayed rapid recovery kinetics during the first part of the recovery curve similar to that of the freely diffusing GFP-NLS, suggesting that a fraction of each protein is free to diffuse within the live cell nucleus. In contrast to GFP-NLS however, both proteins exhibited substantial immobile fractions, which showed no detectable recovery during the time-course of the experiment. This indicates that a substantial fraction of both GFP-MCM2 and GFP-MCM4 is immobile within the live cell nucleus. Our previous work had shown that Cdt1-GFP exhibited short-lived interactions with chromatin which delayed initial fluorescence recovery, leading to a longer $t_{1/2}$ for Cdt1 than the GFP control (47).

Consistent with our earlier findings, Cdt1 exhibited a substantially increased $t_{1/2}$ in comparison to GFP-NLS (Figure 3). Direct comparison of the MCM and Cdt1 FRAP curves shows that MCM proteins exhibit a kinetic behavior which differs significantly from Cdt1: MCM proteins show fast initial recovery and a substantial immobile fraction, while Cdt1 shows reduced initial recovery and a much smaller immobile fraction. We conclude that MCM proteins maintain long-lived interactions within the nucleus in contrast to Cdt1. This is consistent with findings in CHO cells (48) and indicates that the majority of the MCM molecules do not move as a complex with Cdt1 within live human cells.

Imaging MCM dynamics within the nucleus: an in vivo licensing assay - To verify that the observed immobile MCM pool represented MCM- chromatin association during licensing, we investigated whether the presence of an immobile MCM fraction was dependent on Cdt1, a factor essential for the loading of MCM proteins onto chromatin. We therefore knocked down Cdt1 expression in MCF7 cells stable for GFP-MCM2 and GFP-MCM4 using siRNA. The efficiency of the knock-down was assessed by quantitative immunofluorescence (data not shown). As shown in figure 4A, FRAP assays revealed that Cdt1 depletion resulted in significantly reduced immobile fractions for GFP-MCM2 and GFP-MCM4. In contrast, in cells treated with control siRNA, GFP-MCM2 and GFP-MCM4 retained an immobile fraction. We therefore conclude that the presence of an immobile MCM pool is Cdt1 dependent and it is therefore likely to represent MCM-chromatin interactions during licensing.

We then asked whether the observed immobile fraction of MCM proteins is cell cycle regulated, consistent with MCM chromatin binding during licensing. To address this question, GFP-MCM2 and GFP-MCM4 expressing MCF7 cell lines were transiently transfected with proliferating cell nuclear antigen (PCNA) tagged with the red fluorescent protein (RFP). PCNA has been well established as a marker with characteristic cell-cycle dependent nuclear patterns, exhibiting diffuse nuclear distribution in non-S phase cells and subnuclear focal accumulation in S phase cells (Figure 4B). By using this method of discrimination (7), cells at different cell cycle stages were identified and classified according to their pattern of PCNA as non-S, early S, middle S and late S, and analyzed by FRAP. Mean FRAP curves for GFP-MCM2 and GFP-MCM4 are shown in figures 4C and 4D, respectively. In both cases, the recovery half-time ($t_{1/2}$) among the different cell cycle phases is similar and marginally increased compared to GFP-NLS. However, different immobile fractions were observed for both proteins during the course of the cell cycle. Non-S cells demonstrated an immobile fraction of about 22% for GFP-MCM2 and 19% for GFP-MCM4, whereas 30% of GFP-MCM2 and GFP-MCM4 appeared to be immobile in early S phase cells, indicating stable binding of a substantial fraction of MCMs to chromatin at the onset of S phase. In middle to late S phase cells, the immobile fractions were decreased for both GFP-MCM2 and GFP-MCM4, demonstrating that both molecules dissociate from chromatin during the progression through S phase, consistent with licensing loss during S phase.

These findings show that the presence of an immobile MCM pool, as measured by FRAP, closely mirrors MCM-chromatin association during licensing, consistent with earlier work (48). Our assay can therefore be used to assess licensing *in vivo*.

MCM – chromatin association kinetics during the cell cycle reveal increased MCM loading in late G1 phase- We used the *in vivo* licensing assay to study MCM dynamics during the cell cycle of live human cells. Given that the previously analyzed non-S phase cell population represents a heterogeneous pool of cells in different stages of G1 as well as in G2 phase, we investigated MCM kinetic parameters exclusively during G1 phase and examined whether the association of MCM with chromatin changes as G1 phase progresses. To that end, MCF7 cells expressing GFP-MCM2 or GFP-MCM4 were first synchronized in G2/M phase by nocodazole block and mitotic shake-off treatment, released into fresh medium and analyzed as they progressed synchronously through G1. The efficiency of the synchronization was verified by immunofluorescence using cell cycle markers (data not shown), showing that S-phase entry occurred at 12-15 hours following nocodazole release. Cells were analyzed by FRAP at 3 hours (early G1 phase) and 9 hours (middle to late G1 phase) after release. As depicted in figures 5A and 5B, both GFP-MCM2 and GFP-MCM4

exhibited a measurable immobile fraction already from early G1 (3 hours after nocodazole release, observed mean immobile fractions of 8% and 9%, respectively), consistent with stable chromatin association taking place for a small fraction of MCM proteins from early G1. In middle to late G1 cells (9 hours after nocodazole release), the immobile fractions increased somewhat to a mean of 12% and 19%, respectively. This increasing trend is indicative of reiterative loading of MCMs onto chromatin during the course of G1 phase.

Given the significant immobile fraction observed in early S phase cells through co-transfection with PCNA (Figures 4C and 4D), we wished to directly compare MCM - chromatin association kinetics in late G1 with early S phase. For this purpose, MCF7 cell lines expressing either GFP-MCM2 or GFP-MCM4 were arrested in late G1 by treatment with mimosine and in early S phase by hydroxyurea or by double thymidine block. The efficiency of the arrest and the ability of cells to be released from each block were verified by immunofluorescence with specific cell cycle markers (PCNA, Geminin and cyclin A, data not shown). FRAP analysis showed that both GFP-MCM2 and GFP-MCM4 exhibited the largest mean immobile fraction in late G1 (mimosine block, ~25-30%) while immobile fractions for both proteins were considerably lower in the early S phase blocks when compared to late G1 cells (Figures 5C and 5D). To verify that maximal loading of MCM proteins takes place in late G1 phase, MCF7 cells stably expressing GFP-MCM2 or GFP-MCM4 were synchronized in prometaphase by monastrol, which allows reversible mitotic arrest with synchronous entry into the following S phase upon release. BrdU incorporation and staining for Cdt1 was used to characterize progression through the cell cycle and showed that entry into S phase occurred synchronously 15 hours post release from monastrol. Therefore, cells analyzed by FRAP at 3 hours, 7 hours and 13 hours post release were considered to be in early, middle and late G1 phase, respectively. As shown in figures 5E and 5F, both GFP-MCM2 and GFP-MCM4 proteins exhibit maximal loading in late G1 phase (13 hours post release from monastrol) with substantially increased immobile fractions (~30-40%) as compared to early and middle G1 phase (~15%). Taken together, these observations clearly indicate that while a fraction of MCM proteins is loaded onto chromatin from early G1 phase, the majority of MCM proteins are loaded in late G1 phase, prior to the onset of DNA replication.

MCM proteins exhibit dynamic interactions with chromatin during telophase - Our *in vivo* data so far indicates that MCM proteins maintain long-lived interactions with chromatin throughout G1, with maximal chromatin association prior to the G1 to S phase transition. *In vitro* studies have shown that MCM protein loading takes place in two phases, with an initial transient association being converted to stable loading accompanied by ATP hydrolysis and dissociation of MCM loading factors. We therefore wished to investigate if we could detect such a transient MCM-chromatin association early in the cell cycle. Towards this aim, we studied cells in mitosis. We first characterized MCM co-localization with chromatin throughout mitosis. MCF7 cells stable for GFP-MCM4 were synchronized in G2/M with nocodazole, fixed at different time-points after the release and counterstained with DAPI to visualize chromatin. Cells in different stages of mitosis were identified. As shown in figure 6A, MCM4 appeared to be excluded from chromosomes during prophase, metaphase and anaphase. In contrast, MCM4 was shown to overlap with DAPI-stained chromatin in cells undergoing telophase, as nuclear envelopes are reforming. This is similar to the behavior of Cdt1 during mitosis (47). Similar results were obtained for GFP-MCM2 (data not shown).

To elucidate the chromatin association properties of MCMs during the different stages of mitosis, MCF7 cells stably expressing GFP-MCM2 or GFP-MCM4 were transiently transfected with H2B-RFP, a protein that is stably associated with chromatin enabling the observation of chromatin *in vivo*. Cells were then synchronized in mitosis by nocodazole and mitotic shake-off, and time-points taken following release from the drug. Based on the pattern of H2B-RFP, cells were classified into different mitotic phases and subjected to FRAP analysis. Qualitative analysis of the obtained data revealed no immobile fractions and fast fluorescence recovery in the bleached region for both MCM2 and MCM4 in cells in prophase, metaphase and anaphase. On the contrary, the kinetic behavior of MCM2 and

MCM4 was markedly different in cells in telophase (Figures 6B and 6C). In these cells, although no immobile fraction was observed, the initial recovery was much slower (MCM2 $t_{1/2}$ = 0.98 ± 0.09 sec and MCM4 $t_{1/2}$ = 0.84 ± 0.2 sec). The kinetic behavior of MCM proteins in telophase is similar to Cdt1 and differs from MCM kinetics during G1. As shown in Figure 6D, the mobility of GFP-NLS used as control is largely unchanged during mitosis, with only a marginal decrease in mobility in telophase, in contrast to the pronounced retardation observed for GFP-MCM2 and GFP-MCM4. Taken together, these data indicate that in late mitosis MCM proteins maintain transient interactions with chromatin, which are converted to stable interactions from early G1. We conclude that the two steps of MCM loading observed *in vitro*, transient association and stable loading, are separable by FRAP in live cells and transient interactions are only observable for a short window during telophase.

FLIP reveals the spatial distribution of MCM proteins bound to chromatin - FRAP allowed an assessment of the timing and dynamics of MCM - chromatin association in live human cells. In order to address where within the nucleus chromatin association takes place and whether the topology of MCM-chromatin binding changes during the cell cycle, we employed FLIP. MCF7 cells expressing GFP-MCM2 were arrested either in mitosis by nocodazole treatment and then released to enter G1 phase, or in late G1 by mimosine. Cells in early G1 (3 hours after nocodazole release), in middle G1 (7 hours after nocodazole release) or in late G1 (mimosine block) were analyzed by FLIP. During FLIP, a region in the cell nucleus was bleached continuously in order to erase the fluorescence of the mobile fraction of GFP-MCM2. Upon completion of the bleaching pulses, cells were imaged and examined for immobile structures of GFP-MCM2. Representative images are shown in figure 7A. Inspection of the post - FLIP cells revealed discrete GFP-MCM2 assemblies within the nucleus. In early G1, GFP-MCM2 immobile molecules were concentrated in the nuclear periphery and around the nucleoli, reminiscent of heterochromatin localization. The same pattern was retained in middle G1, but in that case the foci were more intense, indicating that a higher percentage of GFP-MCM2 molecules were bound to chromatin. Finally, in late G1 (mimosine block) the relative proportion of GFP-MCM2 bound molecules was even higher and immobile structures were also observed throughout the nucleoplasm (Figure 7A). In order to repeat our analysis using a different synchronization method, cells expressing GFP-MCM2 were arrested in mitosis with monastrol and released to progress synchronously through G1 phase. Cells were analyzed by FLIP 3 hours (early G1), 8 hours (middle G1) and 13 hours (late G1) after the removal of monastrol. As depicted in Figure 7B, analysis of the post-FLIP images showed that in early and middle G1 phase there is a small fraction of GFP-MCM2 molecules that remains bound to chromatin and is predominantly concentrated in the heterochromatic regions. However, in late G1, the immobile fraction of the GFP-MCM2 molecules is substantially higher and immobile structures are observed throughout the nucleus as well as in heterochromatin (Figure 7B), verifying our initial observations. In order to quantify the fraction of GFP-MCM2 molecules that remained bound to chromatin in early, middle and late G1 phase cells, the integrated intensity of the non-bleached part of the nucleus was measured before and after the bleach pulse in 10, 12 and 13 individual cells analyzed by FLIP in early, middle and late G1, respectively (data not shown). The post-bleach over the pre-bleach value was calculated to determine the immobile fractions of the GFP-MCM2 molecules. The immobile GFP-MCM2 fraction is larger in late G1 cells (Mean Imm. Frac. = 0.53 ± 0.23) than in early and middle G1 cells (Mean Imm. Frac. = 0.22 ± 0.16, data not shown). Statistical analysis of the results showed that this difference is highly statistically significant (t-test $p<0.001$). These data further support maximal loading of MCM proteins in late G1, as previously observed by FRAP. They also indicate that MCM-chromatin association is not homogeneous through the nucleus but shows subnuclear concentrations throughout G1.

MCM foci do not colocalize with replication factories - We next monitored changes in MCM chromatin binding at the subnuclear level through S phase by FLIP. To this end, MCF7 cells expressing GFP-MCM2 were transiently transfected with PCNA-RFP, which marks sites of active DNA replication. Using this approach, cells

in early, middle or late S phase were identified and subjected to FLIP (Figure 7C). Under these conditions, the fluorescence of the mobile pool of GFP-MCM2 was depleted whereas GFP-MCM2 molecules that were tightly anchored to chromatin remained unbleached and thus visible. Post-FLIP images revealed that bound GFP-MCM2 molecules were concentrated in subnuclear foci predominantly in early S cells and to a lesser extent in middle S cells. In early S phase, large MCM2 foci were restricted in heterochromatic regions around the nucleus and at the nucleolar periphery. In middle S, although these structures retained their localization, they were fewer and smaller in size. On the contrary, no immobile fraction of GFP-MCM2 was detected during late S phase. Similar results were obtained for GFP-MCM4 (data not shown). These observations are in line with the FRAP results of figures 4C and 4D, providing further support for the gradual loss of MCM immobile fraction during the course of S phase.

Several studies have shown that MCMs do not colocalize with sites of DNA synthesis (32,33,48,57-59). We directly compared the localization of GFP-MCM2 structures and PCNA foci after photobleaching soluble molecules by FLIP. As shown in figure 7B, GFP-MCM2 foci failed to coincide spatially with PCNA, which labels sites of DNA replication, consistent with previous studies (32,33,58). Moreover, PCNA appeared to be in close proximity to GFP-MCM2 foci.

To determine the relative time that MCMs proteins reside on chromatin, the localization of chromatin - bound MCM proteins was imaged for different times following FLIP. MCF7 cells expressing GFP-MCM2 were transiently transfected with PCNA-RFP. Subsequently, cells in G1, early S and middle S phase were selected and subjected to FLIP. Following FLIP, a series of 10 images along the z-axis (z-stacks) were acquired for each cell. The z-stacks, which were collected every 5 minutes over a 2 hour period, were collapsed into maximum intensity projection images and 2D fluorescent intensity versus space mesh plots were generated (Figure 8A). A subnuclear area surrounding GFP-MCM2 foci was defined in each cell and the mean intensity of the specified region was plotted over time to ensure that the total intensity remained constant throughout the experiment and that the repeated imaging caused no significant recording bleaching (Figure 8B). The residence time of GFP-MCM2 molecules on chromatin was estimated by plotting the standard deviation of the per pixel fluorescence intensity within the defined region, as a function of time (Figure 8C). As shown in figure 8C, following FLIP the high standard deviation of per pixel fluorescence intensity observed arises from regions with high levels of bound GFP-MCM2. The standard deviation decreased over time, reflecting the dissociation of GFP-MCM2 molecules from chromatin which move and diffuse within the cell nucleus. As shown in figure 8C, the reduction in standard deviation of the intensity reached a minimum value within 60-80 minutes after FLIP. This observation indicates that GFP-MCM2 resides on chromatin for approximately one hour. No significant difference was detected in the residence time of GFP-MCM2 molecules in cells in G1, early S and middle S phases (Figure 8C).

DISCUSSION

We use here a real-time *in vivo* licensing assay to study in time and space the dynamic behavior of MCM proteins within live human cancer cells. Our analysis reveals distinct modes of MCM interactions with chromatin through the cell cycle: transient interactions in late mitosis are converted to stable binding during G1, while significantly increased loading is apparent close to the G1 to S phase transition followed by loss of interactions during S phase.

A licensing assay in live human cells - Functional imaging was used to assess dynamics of MCM proteins within live human cells. The suitability of the approach to accurately report on the interactions of MCM proteins within cells was verified by several observations. Correct localization and expression levels comparable to the respective endogenous proteins were shown for the GFP tagged MCM proteins used, while cell lines stably expressing the GFP tagged MCM proteins exhibited similar cell cycle profiles to that of parental MCF7 cells. MCM2 and MCM4 GFP-tagged proteins co-fractionated with chromatin in close match to the endogenous proteins and formed complexes with endogenous MCM subunits. FRAP data analysis revealed an

immobile fraction for MCM proteins at cell cycle stages when chromatin is licensed for replication (G1 and early S phase). Importantly, siRNA mediated depletion of Cdt1, a central licensing factor required for the loading of MCMs onto chromatin during G1, resulted in decreased immobile fractions for both GFP-MCM2 and GFP-MCM4 as compared to control siRNA treated cells. Taken together, these observations illustrate that mobility assessed by FRAP indeed reflects the binding of MCMs to chromatin in human cultured cells. Thus, live cell imaging analysis permits the study of the binding properties of MCM proteins with native chromatin in intact living human cells, serving as a molecular tool for the measurement of DNA licensing with high spatio-temporal resolution.

Multi-step loading of MCM proteins to chromatin - Our analysis showed that MCM interactions with chromatin within live cells take place in multiple distinct steps. In early mitosis and up to anaphase, no association of MCM proteins with chromatin is observed and MCM proteins apparently freely diffuse within the cell nucleus, with kinetics comparable to free GFP. During telophase and as a nuclear envelope reforms, retardation in GFP-MCM2 and GFP-MCM4 recovery becomes apparent, indicating transient association with chromatin. Recovery is however complete within a few seconds, suggesting that there is no stably bound component. This is paralleled by the behavior of Cdt1 which appears free to diffuse and excluded from chromatin up to anaphase and exhibits transient interactions with chromatin in telophase (47). In contrast to Cdt1 however, which maintains transient interactions with chromatin throughout G1, both GFP-MCM2 and GFP-MCM4 exhibit an immobile fraction and elevated rate of recovery of the mobile fraction during G1 and S phases, with the time of 50% fluorescence recovery ($t_{1/2}$) ranging from 0,2 - 0,3 sec compared with 0,8 - 1 sec in telophase, respectively. We speculate that during telophase, MCM proteins exchange dynamically on and off chromatin, probing continuously the genome to find appropriate binding sites. Upon entering G1, MCM proteins alter kinetic properties and a fraction of them becomes stably bound to chromatin. The stably bound fraction of MCM proteins increases throughout G1, suggestive of reiterative licensing. Maximal loading is observed at the end of the G1 phase, just prior to the G1 to S phase transition. The bound fraction of MCM proteins becomes gradually lost during S phase, consistent with loss of licensing as DNA is replicated. The binding of MCM proteins to chromatin during G1 appears highly stable, consistent with previous studies (48). We have estimated an apparent residence time of 1-2 hours based on FLIP analysis, while earlier work indicated even longer residence times for MCM proteins in Chinese Hamster Ovary cells (48). In contrast, other components of the pre-replication complex, such as ORC (45) and Cdt1 (46,47), dissociate completely from chromatin within seconds or minutes. This is consistent with *in vitro* work in *Xenopus* egg (60) and yeast extracts (61,62), which showed that the MCM hexamer can be stably loaded on chromatin, while ORC and Cdt1 can be subsequently washed away.

MCM recruitment can be separated from loading during late mitosis - *In vitro* studies in yeast have shown MCM loading onto chromatin to take place in two steps: initial recruitment is converted to stable loading following ATP hydrolysis (36-38).We show here that in human cells MCM proteins interact transiently with chromatin during telophase, exhibiting kinetics similar to Cdt1. This is consistent with MCM recruitment taking place during late mitosis. A transiently interacting MCM component was not detected during G1 phase. A likely explanation for our inability to detect a transiently interacting MCM component during G1, despite indications for re-iterative licensing, is that during the G1 phase recruitment of MCM proteins may be a brief intermediate step that quickly converts to stable loading and therefore a transiently interacting fraction is not detectable. In contrast, during late mitosis, stable loading of MCM proteins onto chromatin may not yet be permitted, and MCM proteins may be trapped in a transiently interacting state for a brief time-window, allowing dynamic associations to be revealed. Post-translational modifications of MCM proteins or other pre-replicative complex subunits could result in trapping the MCM complex in a recruited but not yet loaded state during telophase. It is interesting to note that both MCM4 and Cdt1 appear hyper-phosphorylated in mitosis and early G1 ((55) and

Figure 2). It is also intriguing that during telophase and early G1, chromosome territories within the nucleus are established, in parallel with establishment of the timing of origin firing in the next S phase (10).

Work in fission yeast suggested that the temporal pattern of DNA licensing may determine and reflect the replication timing of DNA origins. MCM proteins were shown to bind early firing origins earlier in G1 compared to late firing origins (63). Using FLIP, we observed accumulation of MCMs at late replicating heterochromatic regions from early G1 in human cells (3 hours post mitotic release) and throughout the G1 phase, in line with previous studies on fixed cells (64). This suggests that if such a differential timing of MCM association with late replicating regions takes place in human cells it is confined to mitotic exit and very early G1 phase.

The majority of MCM proteins are loaded onto chromatin in late G1 phase - Maximal binding of MCM proteins with chromatin was observed late in G1, close to the G1 to S phase transition by both FRAP and FLIP analysis. While a small fraction of MCM proteins are stably bound to chromatin from early G1 phase (around 15%), 30-50% of the molecules are bound just prior to S-phase onset. While we cannot exclude that maximal binding is due to a gradual loading of MCM proteins during the course of G1, our data are more consistent with a wave of MCM chromatin loading or stabilization of MCM proteins on chromatin, preceding S phase entry. A wave of MCM loading could for example be enhanced through cyclin E - mediated protection of cdc6 from proteolysis (65) after the restriction point, while a stabilization of MCM proteins on chromatin could be linked to a decrease in Cdt1 protein levels close to the G1 to S phase transition (50). Our data suggest that while licensing initiates at the end of mitosis, chromatin remains under-licensed until late in G1 phase, close to the G1 to S-phase transition. As premature entry into S phase and under-licensing have been linked to DNA replication stress (24), gaining insight into the events which control multi-step MCM loading is important and will be facilitated by the functional assays presented here.

During S phase, MCM proteins appear to mark unreplicated DNA regions, consistent with previous experiments with fixed (32,33,58) and live (48) cells. The gradual loss of MCM foci as S phase progresses supports the notion that during the process of DNA replication, the DNA replication machinery destabilizes and displaces MCM hexamers from chromatin. Moreover, we observed that the distribution of MCM foci in each phase resembles the characteristic pattern of PCNA of the following phase, in agreement with previous studies performed on fixed cells. In middle S phase, as heterochromatic regions around the nucleoli and at the nuclear periphery were being replicated, MCM foci were distinct from but in close proximity to PCNA foci. Previous analyses showed that new replication factories tend to form adjacent to the ones that recently disassembled (8). Close proximity of active replication factories to high concentrations of licensed origins could contribute to recruitment of released replication factors to these adjacent regions, consistent with a "domino" model of replication factory propagation (9).

In addition to providing insight into the molecular mechanisms involved and the dynamics of DNA licensing within the mammalian cell nucleus, the assays described here are of potential practical utility. For example, the combination of an *in vivo* licensing assay with depletion or overexpression of specific factors may allow the identification of novel factors that block or enhance DNA licensing. Moreover, given that Cdt1/Cdc6 overexpression and thus over-licensing of DNA has been associated with malignant transformation and tumorigenesis, the licensing system has been proposed as a novel molecular target for anti-cancer drug design (23,25). An *in vivo* licensing assay may offer a new approach for cell-based screens for the identification and validation of anti-tumor compounds and drugs under development, that will block DNA licensing and thus DNA replication in cancer cells.

ACKNOWLEDGMENTS
We thank Nickolas Karantzelis, Alexandra Kanellou and Nickolas-Nikiforos Giakoumakis for their advice and assistance. We thank the Advanced Light Microscopy Facility of the University of Patras for help with microscopy. This work was supported by grants from the Association for International Cancer Research and the European Research Council (ERC281851_DYNACOM).

REFERENCES

1. Baker, T. A., and Bell, S. P. (1998) Polymerases and the replisome: machines within machines. *Cell* **92**, 295-305
2. Waga, S., and Stillman, B. (1998) The DNA replication fork in eukaryotic cells. *Annu Rev Biochem* **67**, 721-751
3. Johnson, A., and O'Donnell, M. (2005) Cellular DNA replicases: components and dynamics at the replication fork. *Annu Rev Biochem* **74**, 283-315
4. Symeonidou, I. E., Taraviras, S., and Lygerou, Z. (2012) Control over DNA replication in time and space. *FEBS Lett* **586**, 2803-2812
5. Hozak, P., Hassan, A. B., Jackson, D. A., and Cook, P. R. (1993) Visualization of replication factories attached to nucleoskeleton. *Cell* **73**, 361-373
6. Leonhardt, H., Rahn, H. P., Weinzierl, P., Sporbert, A., Cremer, T., Zink, D., and Cardoso, M. C. (2000) Dynamics of DNA replication factories in living cells. *J Cell Biol* **149**, 271-280
7. Somanathan, S., Suchyna, T. M., Siegel, A. J., and Berezney, R. (2001) Targeting of PCNA to sites of DNA replication in the mammalian cell nucleus. *J Cell Biochem* **81**, 56-67
8. Sporbert, A., Gahl, A., Ankerhold, R., Leonhardt, H., and Cardoso, M. C. (2002) DNA polymerase clamp shows little turnover at established replication sites but sequential de novo assembly at adjacent origin clusters. *Mol Cell* **10**, 1355-1365
9. Chagin, V. O., Stear, J. H., and Cardoso, M. C. (2010) Organization of DNA replication. *Cold Spring Harb Perspect Biol* **2**, a000737
10. Rhind, N., and Gilbert, D. M. (2013) DNA replication timing. *Cold Spring Harb Perspect Biol* **5**
11. Kitamura, E., Blow, J. J., and Tanaka, T. U. (2006) Live-cell imaging reveals replication of individual replicons in eukaryotic replication factories. *Cell* **125**, 1297-1308
12. Blow, J. J., and Dutta, A. (2005) Preventing re-replication of chromosomal DNA. *Nat Rev Mol Cell Biol* **6**, 476-486
13. Nishitani, H., and Lygerou, Z. (2004) DNA replication licensing. *Front Biosci* **9**, 2115-2132
14. Siddiqui, K., On, K. F., and Diffley, J. F. (2013) Regulating DNA Replication in Eukarya. *Cold Spring Harb Perspect Biol*
15. Cocker, J. H., Piatti, S., Santocanale, C., Nasmyth, K., and Diffley, J. F. (1996) An essential role for the Cdc6 protein in forming the pre-replicative complexes of budding yeast. *Nature* **379**, 180-182
16. Maiorano, D., Moreau, J., and Mechali, M. (2000) XCDT1 is required for the assembly of pre-replicative complexes in Xenopus laevis. *Nature* **404**, 622-625
17. Nishitani, H., Lygerou, Z., Nishimoto, T., and Nurse, P. (2000) The Cdt1 protein is required to license DNA for replication in fission yeast. *Nature* **404**, 625-628

18. Masai, H., Matsumoto, S., You, Z., Yoshizawa-Sugata, N., and Oda, M. Eukaryotic chromosome DNA replication: where, when, and how? *Annu Rev Biochem* **79**, 89-130
19. McGarry, T. J., and Kirschner, M. W. (1998) Geminin, an inhibitor of DNA replication, is degraded during mitosis. *Cell* **93**, 1043-1053
20. Wohlschlegel, J. A., Dwyer, B. T., Dhar, S. K., Cvetic, C., Walter, J. C., and Dutta, A. (2000) Inhibition of eukaryotic DNA replication by geminin binding to Cdt1. *Science* **290**, 2309-2312
21. Lygerou, Z., and Nurse, P. (2000) Cell cycle. License withheld--geminin blocks DNA replication. *Science* **290**, 2271-2273
22. Tada, S., Li, A., Maiorano, D., Mechali, M., and Blow, J. J. (2001) Repression of origin assembly in metaphase depends on inhibition of RLF-B/Cdt1 by geminin. *Nat Cell Biol* **3**, 107-113
23. Blow, J. J., and Gillespie, P. J. (2008) Replication licensing and cancer--a fatal entanglement? *Nat Rev Cancer* **8**, 799-806
24. McIntosh, D., and Blow, J. J. (2012) Dormant origins, the licensing checkpoint, and the response to replicative stresses. *Cold Spring Harb Perspect Biol* **4**
25. Petropoulou, C., Kotantaki, P., Karamitros, D., and Taraviras, S. (2008) Cdt1 and Geminin in cancer: markers or triggers of malignant transformation? *Front Biosci* **13**, 4485-4494
26. Adachi, Y., Usukura, J., and Yanagida, M. (1997) A globular complex formation by Nda1 and the other five members of the MCM protein family in fission yeast. *Genes Cells* **2**, 467-479
27. Evrin, C., Clarke, P., Zech, J., Lurz, R., Sun, J., Uhle, S., Li, H., Stillman, B., and Speck, C. (2009) A double-hexameric MCM2-7 complex is loaded onto origin DNA during licensing of eukaryotic DNA replication. *Proc Natl Acad Sci U S A* **106**, 20240-20245
28. Remus, D., Beuron, F., Tolun, G., Griffith, J. D., Morris, E. P., and Diffley, J. F. (2009) Concerted loading of Mcm2-7 double hexamers around DNA during DNA replication origin licensing. *Cell* **139**, 719-730
29. Fletcher, R. J., Bishop, B. E., Leon, R. P., Sclafani, R. A., Ogata, C. M., and Chen, X. S. (2003) The structure and function of MCM from archaeal M. Thermoautotrophicum. *Nat Struct Biol* **10**, 160-167
30. Fu, Y. V., Yardimci, H., Long, D. T., Ho, T. V., Guainazzi, A., Bermudez, V. P., Hurwitz, J., van Oijen, A., Scharer, O. D., and Walter, J. C. (2011) Selective bypass of a lagging strand roadblock by the eukaryotic replicative DNA helicase. *Cell* **146**, 931-941
31. Bell, S. D., and Botchan, M. R. (2013) The Minichromosome Maintenance Replicative Helicase. *Cold Spring Harb Perspect Biol*
32. Dimitrova, D. S., Todorov, I. T., Melendy, T., and Gilbert, D. M. (1999) Mcm2, but not RPA, is a component of the mammalian early G1-phase prereplication complex. *J Cell Biol* **146**, 709-722
33. Krude, T., Musahl, C., Laskey, R. A., and Knippers, R. (1996) Human replication proteins hCdc21, hCdc46 and P1Mcm3 bind chromatin uniformly before S-phase and are displaced locally during DNA replication. *J Cell Sci* **109 (Pt 2)**, 309-318
34. Edwards, M. C., Tutter, A. V., Cvetic, C., Gilbert, C. H., Prokhorova, T. A., and Walter, J. C. (2002) MCM2-7 complexes bind chromatin in a distributed pattern surrounding the origin recognition complex in Xenopus egg extracts. *J Biol Chem* **277**, 33049-33057

35. Mahbubani, H. M., Chong, J. P., Chevalier, S., Thommes, P., and Blow, J. J. (1997) Cell cycle regulation of the replication licensing system: involvement of a Cdk-dependent inhibitor. *J Cell Biol* **136**, 125-135
36. Francis, L. I., Randell, J. C., Takara, T. J., Uchima, L., and Bell, S. P. (2009) Incorporation into the prereplicative complex activates the Mcm2-7 helicase for Cdc7-Dbf4 phosphorylation. *Genes Dev* **23**, 643-654
37. Frigola, J., Remus, D., Mehanna, A., and Diffley, J. F. (2013) ATPase-dependent quality control of DNA replication origin licensing. *Nature* **495**, 339-343
38. Tsakraklides, V., and Bell, S. P. (2010) Dynamics of pre-replicative complex assembly. *J Biol Chem* **285**, 9437-9443
39. Randell, J. C., Bowers, J. L., Rodriguez, H. K., and Bell, S. P. (2006) Sequential ATP hydrolysis by Cdc6 and ORC directs loading of the Mcm2-7 helicase. *Mol Cell* **21**, 29-39
40. Tanaka, S., and Araki, H. (2013) Helicase Activation and Establishment of Replication Forks at Chromosomal Origins of Replication. *Cold Spring Harb Perspect Biol*
41. Moyer, S. E., Lewis, P. W., and Botchan, M. R. (2006) Isolation of the Cdc45/Mcm2-7/GINS (CMG) complex, a candidate for the eukaryotic DNA replication fork helicase. *Proc Natl Acad Sci U S A* **103**, 10236-10241
42. Ilves, I., Petojevic, T., Pesavento, J. J., and Botchan, M. R. Activation of the MCM2-7 helicase by association with Cdc45 and GINS proteins. *Mol Cell* **37**, 247-258
43. Gambus, A., Jones, R. C., Sanchez-Diaz, A., Kanemaki, M., van Deursen, F., Edmondson, R. D., and Labib, K. (2006) GINS maintains association of Cdc45 with MCM in replisome progression complexes at eukaryotic DNA replication forks. *Nat Cell Biol* **8**, 358-366
44. Pacek, M., Tutter, A. V., Kubota, Y., Takisawa, H., and Walter, J. C. (2006) Localization of MCM2-7, Cdc45, and GINS to the site of DNA unwinding during eukaryotic DNA replication. *Mol Cell* **21**, 581-587
45. McNairn, A. J., Okuno, Y., Misteli, T., and Gilbert, D. M. (2005) Chinese hamster ORC subunits dynamically associate with chromatin throughout the cell-cycle. *Exp Cell Res* **308**, 345-356
46. Xouri, G., Dimaki, M., Bastiaens, P. I., and Lygerou, Z. (2007) Cdt1 interactions in the licensing process: a model for dynamic spatiotemporal control of licensing. *Cell Cycle* **6**, 1549-1552
47. Xouri, G., Squire, A., Dimaki, M., Geverts, B., Verveer, P. J., Taraviras, S., Nishitani, H., Houtsmuller, A. B., Bastiaens, P. I., and Lygerou, Z. (2007) Cdt1 associates dynamically with chromatin throughout G1 and recruits Geminin onto chromatin. *Embo J* **26**, 1303-1314
48. Kuipers, M. A., Stasevich, T. J., Sasaki, T., Wilson, K. A., Hazelwood, K. L., McNally, J. G., Davidson, M. W., and Gilbert, D. M. (2011) Highly stable loading of Mcm proteins onto chromatin in living cells requires replication to unload. *J Cell Biol* **192**, 29-41
49. Pefani, D. E., Dimaki, M., Spella, M., Karantzelis, N., Mitsiki, E., Kyrousi, C., Symeonidou, I. E., Perrakis, A., Taraviras, S., and Lygerou, Z. Idas, a novel phylogenetically conserved geminin-related protein, binds to geminin and is required for cell cycle progression. *J Biol Chem*
50. Nishitani, H., Taraviras, S., Lygerou, Z., and Nishimoto, T. (2001) The human licensing factor for DNA replication Cdt1 accumulates in G1 and is destabilized after initiation of S-phase. *J Biol Chem* **276**, 44905-44911

51. Mortusewicz, O., Schermelleh, L., Walter, J., Cardoso, M. C., and Leonhardt, H. (2005) Recruitment of DNA methyltransferase I to DNA repair sites. *Proc Natl Acad Sci U S A* **102**, 8905-8909
52. Rapsomaniki, M. A., Kotsantis, P., Symeonidou, I. E., Giakoumakis, N. N., Taraviras, S., and Lygerou, Z. (2012) easyFRAP: an interactive, easy-to-use tool for qualitative and quantitative analysis of FRAP data. *Bioinformatics* **28**, 1800-1801
53. Masai, H., Taniyama, C., Ogino, K., Matsui, E., Kakusho, N., Matsumoto, S., Kim, J. M., Ishii, A., Tanaka, T., Kobayashi, T., Tamai, K., Ohtani, K., and Arai, K. (2006) Phosphorylation of MCM4 by Cdc7 kinase facilitates its interaction with Cdc45 on the chromatin. *J Biol Chem* **281**, 39249-39261
54. Kimura, H., Ohtomo, T., Yamaguchi, M., Ishii, A., and Sugimoto, K. (1996) Mouse MCM proteins: complex formation and transportation to the nucleus. *Genes Cells* **1**, 977-993
55. Nishitani, H., Lygerou, Z., and Nishimoto, T. (2004) Proteolysis of DNA replication licensing factor Cdt1 in S-phase is performed independently of geminin through its N-terminal region. *The Journal of biological chemistry* **279**, 30807-30816
56. Ishimi, Y., and Komamura-Kohno, Y. (2001) Phosphorylation of Mcm4 at specific sites by cyclin-dependent kinase leads to loss of Mcm4,6,7 helicase activity. *J Biol Chem* **276**, 34428-34433
57. Laskey, R. A., and Madine, M. A. (2003) A rotary pumping model for helicase function of MCM proteins at a distance from replication forks. *EMBO Rep* **4**, 26-30
58. Romanowski, P., Madine, M. A., and Laskey, R. A. (1996) XMCM7, a novel member of the Xenopus MCM family, interacts with XMCM3 and colocalizes with it throughout replication. *Proc Natl Acad Sci U S A* **93**, 10189-10194
59. Todorov, I. T., Attaran, A., and Kearsey, S. E. (1995) BM28, a human member of the MCM2-3-5 family, is displaced from chromatin during DNA replication. *J Cell Biol* **129**, 1433-1445
60. Rowles, A., Tada, S., and Blow, J. J. (1999) Changes in association of the Xenopus origin recognition complex with chromatin on licensing of replication origins. *J Cell Sci* **112 (Pt 12)**, 2011-2018
61. Bowers, J. L., Randell, J. C., Chen, S., and Bell, S. P. (2004) ATP hydrolysis by ORC catalyzes reiterative Mcm2-7 assembly at a defined origin of replication. *Mol Cell* **16**, 967-978
62. Donovan, S., Harwood, J., Drury, L. S., and Diffley, J. F. (1997) Cdc6p-dependent loading of Mcm proteins onto pre-replicative chromatin in budding yeast. *Proc Natl Acad Sci U S A* **94**, 5611-5616
63. Wu, P. Y., and Nurse, P. (2009) Establishing the program of origin firing during S phase in fission Yeast. *Cell* **136**, 852-864
64. Dimitrova, D. S., Giacca, M., Demarchi, F., Biamonti, G., Riva, S., and Falaschi, A. (1996) In vivo protein-DNA interactions at human DNA replication origin. *Proc Natl Acad Sci U S A* **93**, 1498-1503
65. Mailand, N., and Diffley, J. F. (2005) CDKs promote DNA replication origin licensing in human cells by protecting Cdc6 from APC/C-dependent proteolysis. *Cell* **122**, 915-926

FIGURE LEGENDS

FIGURE 1. Characterization of MCF7 cells stably expressing GFP-MCM2, GFP-MCM4 or GFP-NLS. A. GFP-MCM2 and GFP-MCM4 proteins are expressed at levels similar to endogenous. Total cell extracts from parental MCF7 cells and cells stably expressing GFP-NLS, GFP-MCM2 or GFP-MCM4 were analyzed by western blotting using antibodies against MCM2, MCM4, GFP and tubulin as loading control. B, C. GFP-MCM2 and GFP-MCM4 proteins are confined to the nucleus and are absent from the nucleoli. Parental MCF7 cells and cells stably expressing GFP-MCM2, GFP-NLS or GFP-MCM4 as indicated, were analyzed by immunofluorescence using antibodies against MCM2 (B) or MCM4 (C), respectively. DNA was stained with TOTO-3. D, E. Stable cells exhibit a physiological cell cycle profile. Cells were fixed, stained with propidium iodide and subjected to FACS analysis (D) or immunostained with antibodies against Cdt1, Geminin or Cyclin A and the number of cells positive for each staining was recorded (E). F. GFP-MCM2 and GFP-MCM4 form complexes with endogenous MCM proteins. Extracts from parental MCF7, stable GFP-NLS, GFP-MCM2 and GFP-MCM4 cells were prepared, immunoprecipitated using an antibody against GFP and immunobloted with antibodies against GFP, MCM2, MCM4 and MCM7.

FIGURE 2. GFP-MCM2 and GFP-MCM4 bind to chromatin during G1 phase, similar to endogenous MCM2 and MCM4 proteins. A, B. Stable GFP-MCM2 (A) and GFP-MCM4 (B) cells were synchronized in M phase by nocodazole block and mitotic shake-off and cells were harvested at different time points (40, 50, 150, 300 and 600 minutes) as they progressed into G1 phase. Total cell extracts were prepared (Total) and further fractionated into a soluble (S100) and a chromatin - enriched fraction (P100) (see Experimental Procedures). Fractions were subjected to western blot analysis using antibodies against MCM2, MCM4, Cdt1. Tubulin and Commassie Brilliant Blue staining (CBB) were used as loading controls.

FIGURE 3. Fluorescence Recovery after Photobleaching shows GFP-MCM2 and GFP-MCM4 dynamics in live cells. Asynchronous MCF7 cells stably expressing GFP-MCM2, GFP-MCM4, Cdt1-GFP or GFP-NLS were analyzed by FRAP. Recovery of fluorescence in the photobleached region as a function of time is depicted. Immobile fraction (Imm. Frac.) and half-time ($t_{1/2}$) of the recovery of the mobile fraction were calculated for each curve, after fitting the data as described in Experimental Procedures using easyFRAP (52). N represents the number of cells analyzed in each condition. Mean values are given for the calculated immobile fraction and half-time of recovery, with corresponding standard deviations.

FIGURE 4. GFP-MCM2 and GFP-MCM4 bind to chromatin in a Cdt1-dependent manner and exhibit different binding properties through the cell cycle. A. Stable GFP-MCM2, GFP-MCM4 and GFP-NLS cells were treated with non target siRNA (siLuc) or siRNA for Cdt1 (siCdt1) followed by FRAP analysis. B. PCNA localization enables discrimination of different cell cycle phases. Stable GFP-MCM4 cells transiently transfected with PCNA-RFP were fixed and representative images of characteristic non-S and S phase patterns (early S, middle S and late S) were taken. C and D. Stable GFP-MCM2 (C), GFP-MCM4 (D) and GFP-NLS cells were transiently transfected with PCNA-RFP. Cells in early, middle and late S-phase, as well as non-S-phase cells were identified based on the localization of PCNA and analyzed by FRAP. Recovery of fluorescence in the photobleached region as a function of time is depicted. Mean values are given for the calculated immobile fraction and half-time of recovery for all conditions tested, with corresponding standard deviations. N represents the number of cells analyzed for each condition.

FIGURE 5. GFP-MCM2 and GFP-MCM4 display maximal binding to chromatin during late G1 phase. A, B. Stable GFP-MCM2 (A) and GFP-MCM4 (B) cells were synchronized in M phase by nocodazole block and mitotic shake off. GFP-MCM2/4 cells in early G1 (3 hours post mitotic release) and in middle to late G1 (9 hours post mitotic release), as well as unsynchronized stable Cdt1-GFP and GFP-NLS cells were analysed by FRAP. C, D. Stable GFP-MCM2 (C) and GFP-MCM4 (D) cells were synchronized in

late G1 after mimosine treatment (mimosine), and in early S phase by a double thymidine block (thymidine) or hydroxurea (HU) treatment and analysed by FRAP, in parallel to unsynchronized GFP-MCM2/4 and GFP-NLS cells. E, F. Stable GFP-MCM2 (E) and GFP-MCM4 cells were synchronized in mitosis by monastrol and time points taken in early, middle and late G1 phase (at 3, 7 and 13 hours following release). Recovery of fluorescence in the photobleached region as a function of time is depicted for all conditions. G, H. Following curve fitting of individual FRAP curves, immobile fraction (Imm. Frac.) and half-time ($t_{1/2}$) of the recovery of the mobile fraction were computed for all cells analyzed in panels A-F using easyFRAP (52). N represents the number of cells analyzed for each condition. Mean values with standard deviation are shown.

FIGURE 6. GFP-MCM2/4 display transient binding during telophase. A. GFP-MCM4 is absent from chromatin during prophase, metaphase and anaphase, but co-localizes with chromatin during telophase. Stable GFP-MCM4 cells were synchronized in M phase after nocodazole block, fixed and DNA was stained with DAPI. B-D. Stable GFP-MCM2 (B) , GFP-MCM4 (C) and control GFP-NLS cells (D) were transiently transfected with a plasmid expressing H2B-RFP which marks chromosomes. Cells in the different stages of M phase were identified based on morphology and analyzed by FRAP. Fluorescence recovery is shown as a function of time. Immobile fraction (Imm. Frac.) and half-time ($t_{1/2}$) of the recovery of the mobile fraction were computed. N represents the number of cells analyzed for each condition.

FIGURE 7. Subnuclear distribution of chromatin - bound GFP-MCM2. A. Stable GFP-MCM2 cells were either synchronized in M phase after nocodazole block and mitotic shake off and released into G1 phase or synchronized in late G1 phase by mimosine treatment. After 3 hours (post noc 3h) and 7 hours (post noc 7h) following nocodazole release and in late G1 phase (mimosine block) cells were subjected to FLIP analysis and representative images are shown before and after the bleaching step. B. Stable GFP-MCM2 cells were synchronized in mitosis by monastrol and released into a synchronous G1 phase. At 3, 7 and 13 hours post release (early, middle and late G1 phase respectively) cells were analyzed by FLIP. Pre and post-bleach images are shown for representative cells. C. GFP-MCM2 does not colocalize with PCNA foci in the various stages of S phase. Stable GFP-MCM2 cells were transiently transfected with PCNA-RFP. Cells were discriminated according to PCNA patterning, FLIP was carried out and representative images were taken. Cells before bleaching are displayed on the left (pre bleach) and cells after bleaching are displayed on the right (post bleach). In all panels, the bleached regions are marked by a red line in the post-bleached images. In panels A and B, red arrowheads indicate immobile structures of GFP-MCM2. In panel C, part of the post-bleach images in early and middle - S cells has been blown up (red squares) to highlight the lack of colocalization between PCNA and GFP-MCM2 foci. The difference in fluorescence intensity between panels A and B is due to differences in recording and bleaching conditions.

FIGURE 8. GFP-MCM2 resides on chromatin for approximately 60 to 80 minutes. A. Stable GFP-MCM2 cells were transiently transfected with a plasmid expressing PCNA-RFP. Cells in G1, early S and middle S phase were identified according to PCNA patterning and subjected to FLIP. Z-stack sections of each cell's volume were captured every 5 minutes for a total duration of 2 hours and mesh plots were created as described in Experimental Procedures. A subnuclear area of each cell containing GFP-MCM2 foci was defined (red boxes) and the fluorescence intensity (B) as well as the corresponding standard deviation (C) were plotted throughout the course of the experiment.

Figure 1

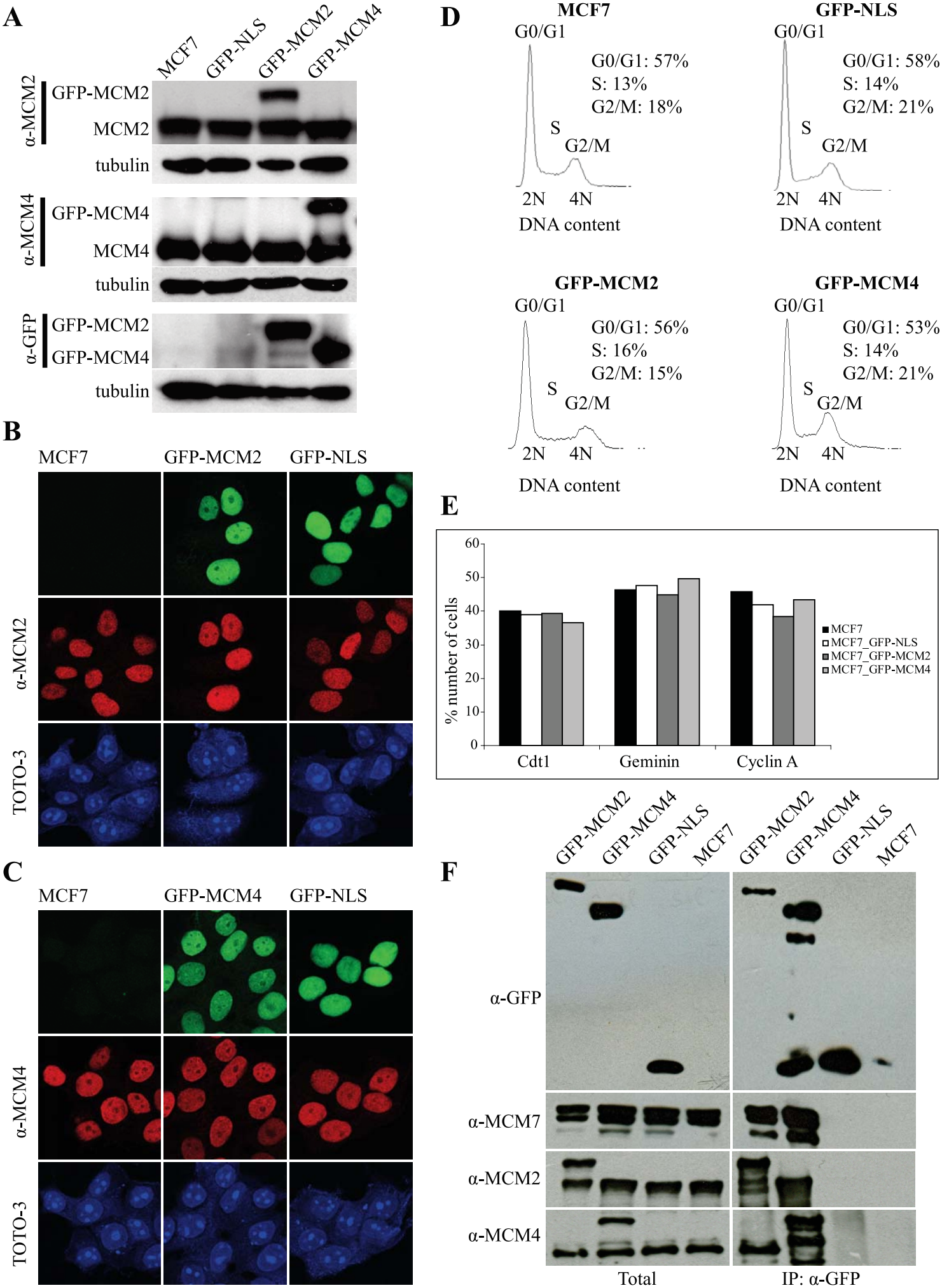
A
MCF7
GFP-NLS
GFP-MCM2
GFP-MCM4
α-MCM2
GFP-MCM2
MCM2
tubulin
α-MCM4
GFP-MCM4
MCM4
tubulin
α-GFP
GFP-MCM2
GFP-MCM4
tubulin
B
MCF7
GFP-MCM2
GFP-NLS
α-MCM2
TOTO-3
C
MCF7
GFP-MCM4
GFP-NLS
α-MCM4
TOTO-3
D
MCF7
G0/G1
G0/G1: 57%
S: 13%
G2/M: 18%
S
G2/M
2N
4N
DNA content
GFP-NLS
G0/G1
G0/G1: 58%
S: 14%
G2/M: 21%
S
G2/M
2N
4N
DNA content
GFP-MCM2
G0/G1
G0/G1: 56%
S: 16%
G2/M: 15%
S
G2/M
2N
4N
DNA content
GFP-MCM4
G0/G1
G0/G1: 53%
S: 14%
G2/M: 21%
S
G2/M
2N
4N
DNA content
E
% number of cells
60
50
40
30
20
10
0
Cdt1
Geminin
Cyclin A
MCF7
MCF7_GFP-NLS
MCF7_GFP-MCM2
MCF7_GFP-MCM4
F
GFP-MCM2
GFP-MCM4
GFP-NLS
MCF7
GFP-MCM2
GFP-MCM4
GFP-NLS
MCF7
α-GFP
α-MCM7
α-MCM2
α-MCM4
Total
IP: α-GFP

Figure 2

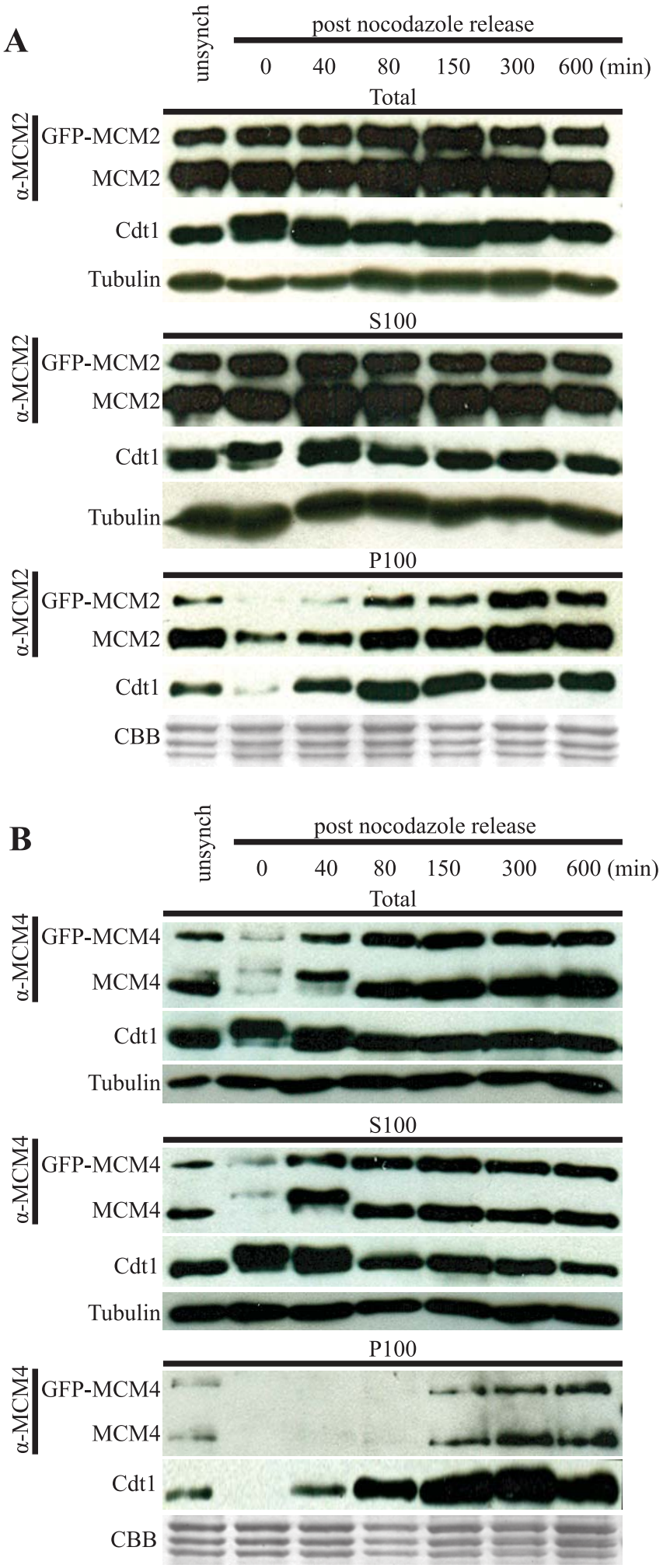
A
unsynch
post nocodazole release
0
40
80
150
300
600 (min)
Total
α-MCM2
GFP-MCM2
MCM2
Cdt1
Tubulin
S100
α-MCM2
GFP-MCM2
MCM2
Cdt1
Tubulin
P100
α-MCM2
GFP-MCM2
MCM2
Cdt1
CBB
B
unsynch
post nocodazole release
0
40
80
150
300
600 (min)
Total
α-MCM4
GFP-MCM4
MCM4
Cdt1
Tubulin
S100
α-MCM4
GFP-MCM4
MCM4
Cdt1
Tubulin
P100
α-MCM4
GFP-MCM4
MCM4
Cdt1
CBB

Figure 3

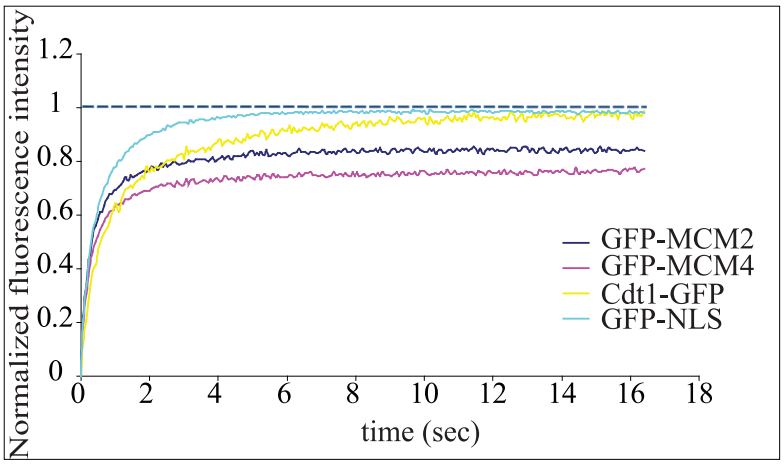

	$t_{1/2}$ (sec)	Imm. Frac.	N
GFP-MCM2	0.23 ± 0.07	0.16 ± 0.15	50
GFP-MCM4	0.23 ± 0.07	0.23 ± 0.2	48
Cdt1-GFP	0.57 ± 0.09	0.03 ± 0.03	15
GFP-NLS	0.29 ± 0.08	0.02 ± 0.02	15

Figure 4

A

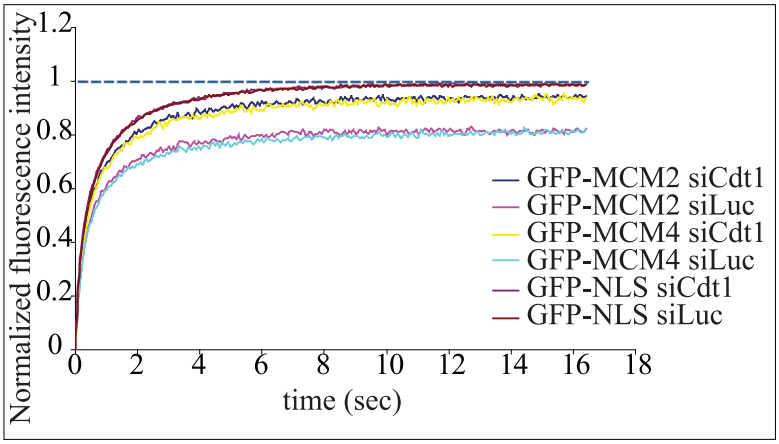

	$t_{1/2}$ (sec)	Imm. Frac.	N
GFP-MCM2 siCdt1	0.35 ± 0.07	0.06 ± 0.09	25
GFP-MCM2 siLuc	0.32 ± 0.08	0.19 ± 0.2	25
GFP-MCM4 siCdt1	0.38 ± 0.1	0.09 ± 0.15	25
GFP-MCM4 siLuc	0.36 ± 0.09	0.2 ± 0.2	25
GFP-NLS siCdt1	0.32 ± 0.07	0.02 ± 0.02	20
GFP-NLS siLuc	0.34 ± 0.1	0.02 ± 0.01	20

B

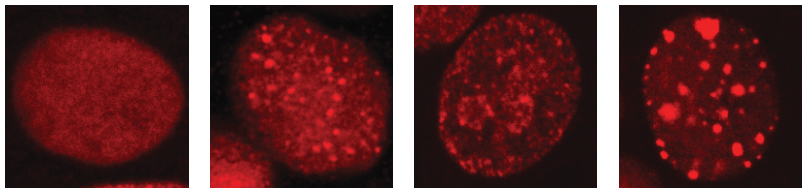

C

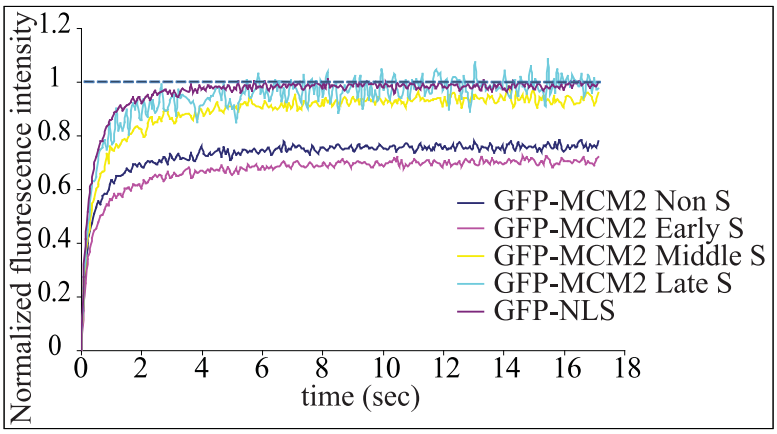

	$t_{1/2}$ (sec)	Imm. Frac.	N
GFP-MCM2 Non S	0.2 ± 0.07	0.22 ± 0.14	23
GFP-MCM2 Early S	0.26 ± 0.08	0.3 ± 0.11	25
GFP-MCM2 Middle S	0.27 ± 0.06	0.07 ± 0.04	10
GFP-MCM2 Late S	0.25 ± 0.04	0.02 ± 0.02	3
GFP-NLS	0.2 ± 0.06	0.02 ± 0.1	6

D

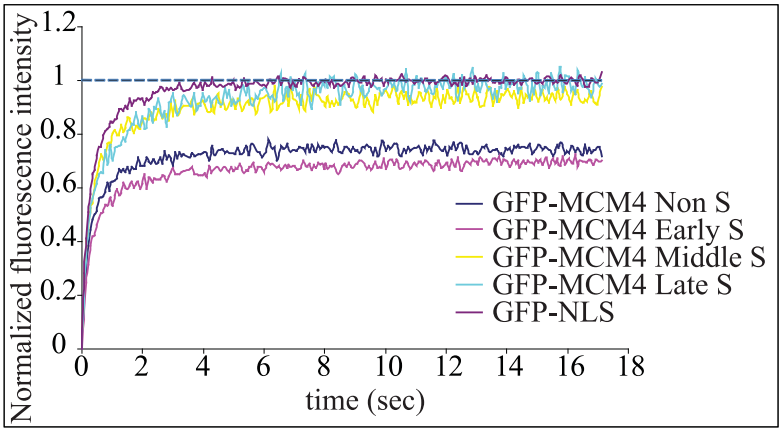

	$t_{1/2}$ (sec)	Imm. Frac.	N
GFP-MCM4 Non S	0.24 ± 0.23	0.19 ± 0.2	23
GFP-MCM4 Early S	0.25 ± 0.09	0.3 ± 0.1	24
GFP-MCM4 Middle S	0.23 ± 0.06	0.06 ± 0.06	11
GFP-MCM4 Late S	0.25 ± 0.08	0.02 ± 0.02	4
GFP-NLS	0.2 ± 0.03	0.01 ± 0.02	10

Figure 5

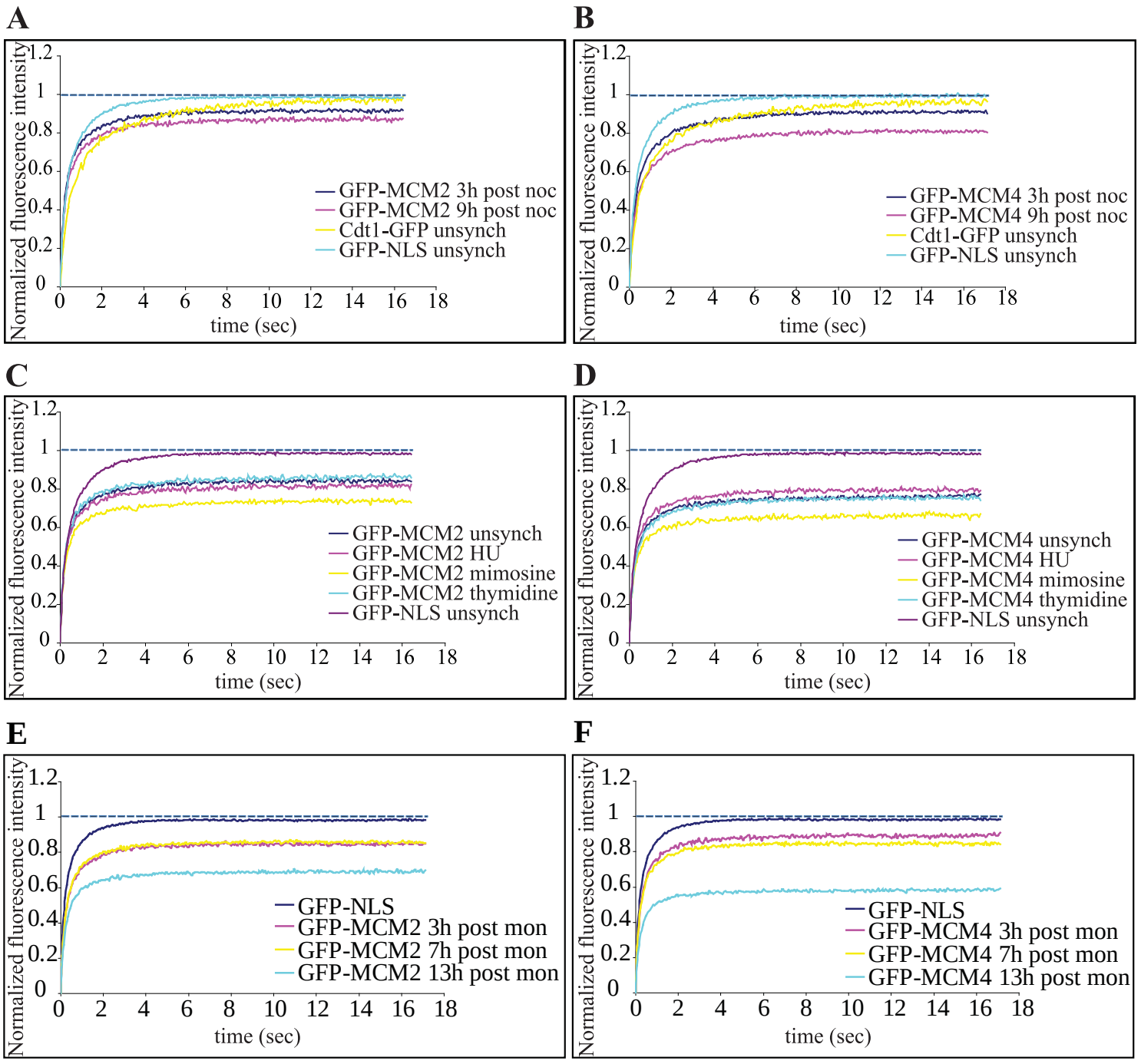

G

		$t_{1/2}$ (sec)	Imm. Frac.	N
Fig 5A	GFP-MCM2 3h p.n.	0.22 ± 0.05	0.08 ± 0.06	40
	GFP-MCM2 9h p.n.	0.23 ± 0.05	0.12 ± 0.13	39
	Cdt1-GFP unsynch	0.52 ± 0.09	0.04 ± 0.04	11
	GFP-NLS unsynch	0.27 ± 0.06	0.01 ± 0.02	10
Fig 5C	GFP-MCM2 unsynch	0.23 ± 0.07	0.16 ± 0.15	50
	GFP-MCM2 HU	0.20 ± 0.06	0.18 ± 0.11	49
	GFP-MCM2 mim	0.19 ± 0.05	0.26 ± 0.11	50
	GFP-MCM2 thym	0.20 ± 0.06	0.13 ± 0.11	49
	GFP-NLS unsynch	0.29 ± 0.08	0.02 ± 0.02	15
Fig 5E	GFP-MCM2 3h p.m.	0.20 ± 0.03	0.15 ± 0.10	30
	GFP-MCM2 7h p.m.	0.21 ± 0.03	0.14 ± 0.12	30
	GFP-MCM2 13h p.m.	0.21 ± 0.04	0.31 ± 0.23	27
	GFP-NLS unsynch	0.16 ± 0.04	0.02 ± 0.02	11

H

		$t_{1/2}$ (sec)	Imm. Frac.	N
Fig 5B	GFP-MCM4 3h p.n.	0.31 ± 0.07	0.09 ± 0.1	31
	GFP-MCM4 9h p.n.	0.32 ± 0.09	0.19 ± 0.15	30
	Cdt1-GFP unsynch	0.52 ± 0.09	0.04 ± 0.04	11
	GFP-NLS unsynch	0.27 ± 0.06	0.01 ± 0.02	10
Fig 5D	GFP-MCM4 unsynch	0.23 ± 0.07	0.24 ± 0.2	48
	GFP-MCM4 HU	0.20 ± 0.05	0.2 ± 0.14	50
	GFP-MCM4 mim	0.20 ± 0.10	0.3 ± 0.15	47
	GFP-MCM4 thym	0.23 ± 0.06	0.25 ± 0.12	50
	GFP-NLS unsynch	0.29 ± 0.08	0.02 ± 0.02	15
Fig 5F	GFP-MCM4 3h p.m.	0.19 ± 0.05	0.11 ± 0.09	34
	GFP-MCM4 7h p.m.	0.18 ± 0.05	0.15 ± 0.13	35
	GFP-MCM4 13h p.m.	0.19 ± 0.05	0.38 ± 0.21	31
	GFP-NLS unsynch	0.16 ± 0.04	0.02 ± 0.02	11

Figure 6

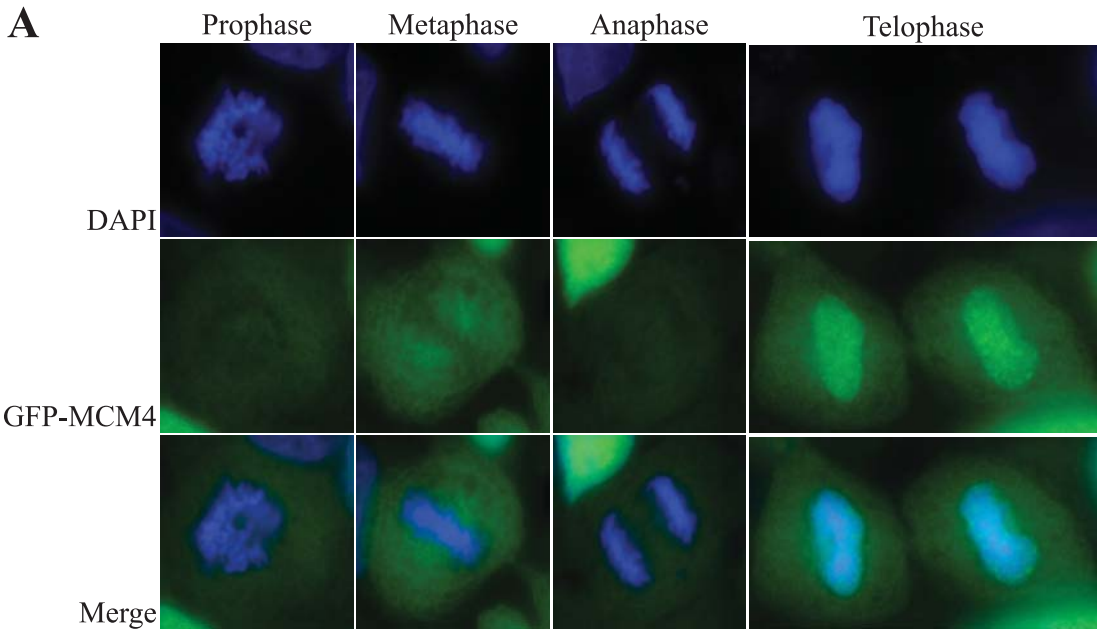

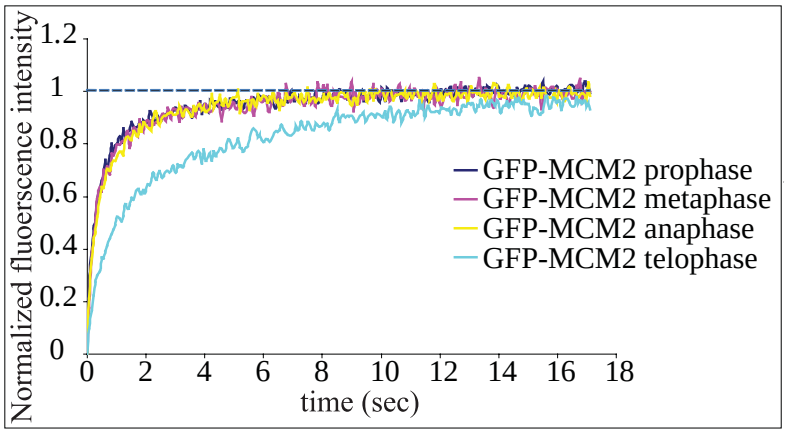

GFP-MCM2	$t_{1/2}$ (sec)	Imm. Frac.	N
prophase	0.28 ± 0.07	0.01 ± 0.01	10
metaphase	0.27 ± 0.08	0.01 ± 0.01	5
anaphase	0.27 ± 0.04	0.01 ± 0.01	4
telophase	0.98 ± 0.09	0.03 ± 0.04	4

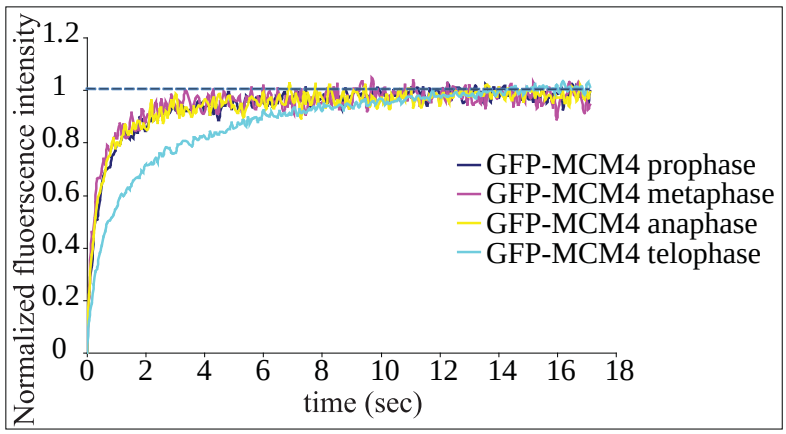

GFP-MCM4	$t_{1/2}$ (sec)	Imm. Frac.	N
prophase	0.31 ± 0.06	0.02 ± 0.02	10
metaphase	0.23 ± 0.11	0.02 ± 0.02	6
anaphase	0.28 ± 0.11	0.02 ± 0.02	7
telophase	0.84 ± 0.20	0.01 ± 0.02	10

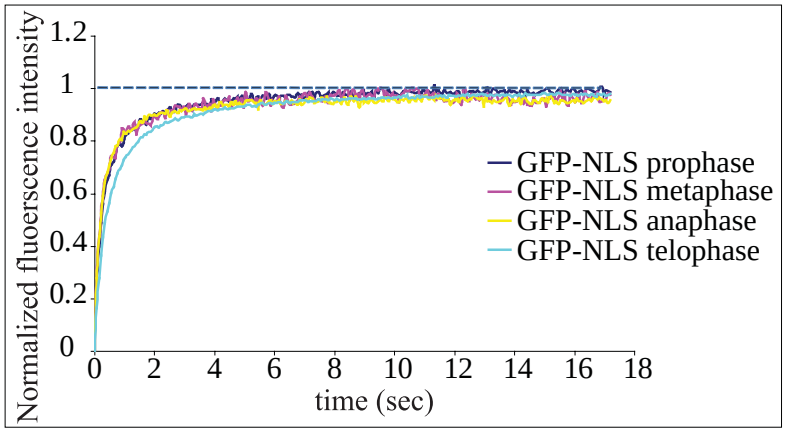

GFP-NLS	$t_{1/2}$ (sec)	Imm. Frac.	N
prophase	0.21 ± 0.04	0.02 ± 0.04	20
metaphase	0.17 ± 0.04	0.04 ± 0.03	7
anaphase	0.17 ± 0.05	0.05 ± 0.06	6
telophase	0.37 ± 0.12	0.03 ± 0.04	18

Figure 7

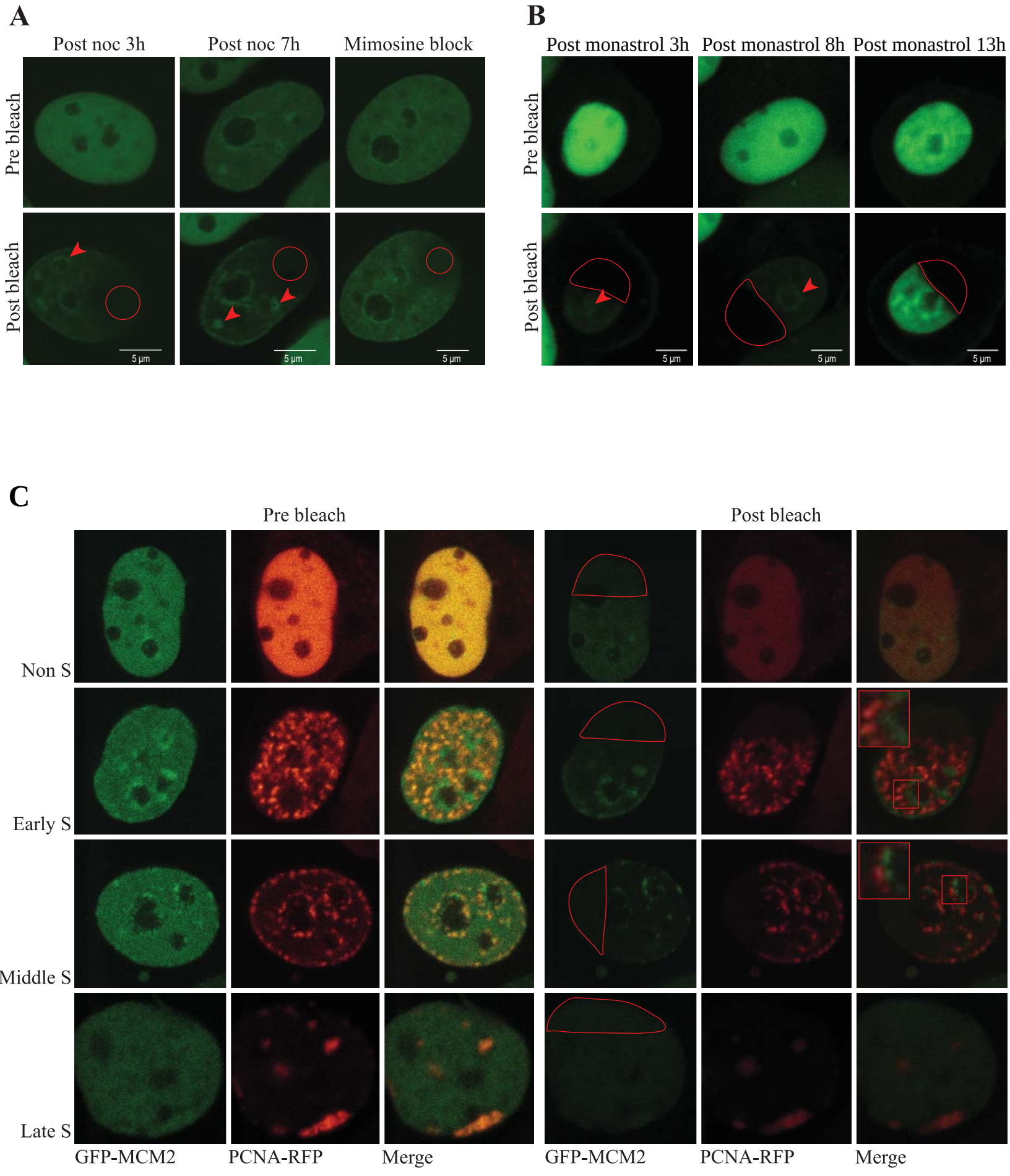
A
Post noc 3h
Post noc 7h
Mimosine block
Pre bleach
Post bleach
5 µm
B
Post monastrol 3h
Post monastrol 8h
Post monastrol 13h
Pre bleach
Post bleach
5 µm
C
Pre bleach
Post bleach
Non S
Early S
Middle S
Late S
GFP-MCM2
PCNA-RFP
Merge
GFP-MCM2
PCNA-RFP
Merge

Figure 8

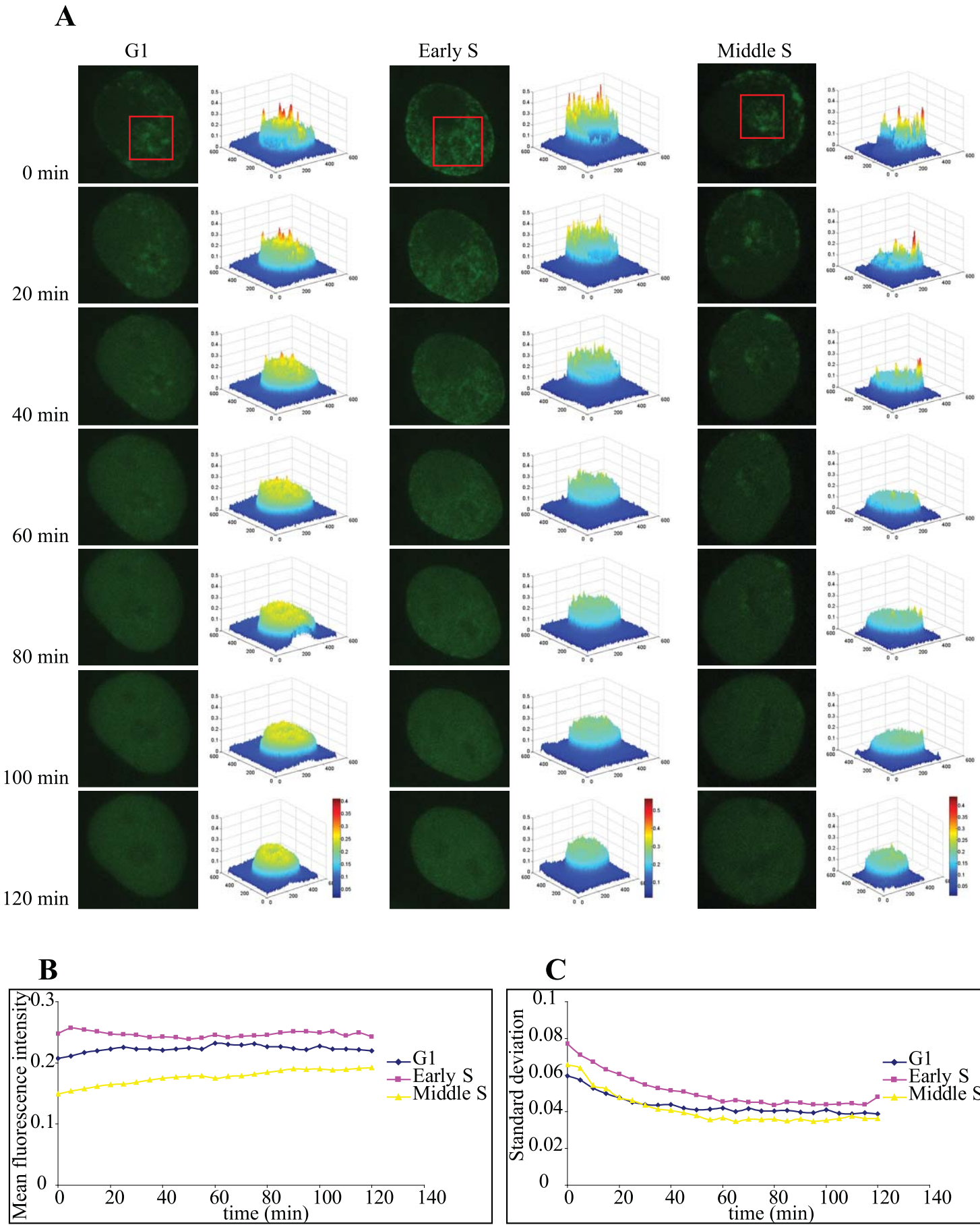
A
G1
Early S
Middle S
0 min
20 min
40 min
60 min
80 min
100 min
120 min
B
Mean fluorescence intensity
0
0.1
0.2
0.3
0
20
40
60
80
100
120
140
time (min)
G1
Early S
Middle S
C
Standard deviation
0
0.02
0.04
0.06
0.08
0.1
0
20
40
60
80
100
120
140
time (min)
G1
Early S
Middle S